THERMAL ANALYSIS OF SINGLE POINT CUTTING TOOL

A thesis Submitted in Partial Fulfilment of the Requirements

For the Degree of

B.Tech

In

Mechanical Engineering

By

ANOHITO CHOPHY (15120409)
ARUN KRISHNAN M U (15120413)
NEERAJ KRISHNA M NAIR (15120441)
PRINCE KURIAKOSE (15120442)
ABDUL SAMAD A (15120463)

MECHANICAL ENGINEERING DEPARTMENT
COLLEGE OF ENGINEERING ADOOR
MANAKALA-691551

APRIL, 2015

BONAFIDE CERTIFICATE

This is to certify that the project titled **"THERMAL ANALYSIS OF SINGLE POINT CUTTING TOOL "**is a bonafide record of the work done by

ANOHITO CHOPHY (15120409)
ARUN KRISHNAN M U (15120413)
NEERAJ KRISHNA M NAIR (15120441)
PRINCE KURIAKOSE (15120442)
ABDUL SAMAD A (15120463)

in partial fulfilment of the requirements for the award of the degree of **Bachelor of Technology** in **Mechanical Engineering** of **COCHIN UNIVERSITY OF SCIENCE AND TECHNOLOGY** at **COLLEGE OF ENGINEERING ADOOR, MANAKALA,** during the year 2014-2015.

Sri. SANCHU S **Sri. MANU M JOHN**
Project Guide Head of the Department

Project Viva-voce held on:

Internal Examiner **External Examiner**

ABSTRACT

Temperature at tool-chip interface of a single point cutting tool is determined, generated in different speed machining operations. Specifically, three different analyses are comparing to an experimental measurement of temperature in a machining process at slow speed, medium speed and at high speed. In addition, three analyses are done of a High Speed Steel and of a Carbide Tip Tool machining process at three different cutting speeds, in order to compare to experimental results produced as part of this study. An investigation of heat generation in cutting tool is performed by varying cutting parameters at the suitable cutting tool geometry. The experimental results reveal that the main factors responsible for increasing cutting temperature are cutting speed (v) and depth of cut (d) respectively. Various researches have been undertaken in measuring the temperatures generated during cutting operations. Investigators made attempt to measure these cutting temperatures with various techniques during machining.

"Fluke IR Thermal Imager" is used for measuring temperature at tool-chip interface. Single point cutting tool has been solid modelled by using SOLIDWORKS 2013 and Finite Element Analysis carried out by using ANSYS Workbench 15. By varying various parameters the effect of those on temperature are compared with the experimental results and FEA results.

Keywords: Single Point Cutting Tool, HSS tool and Carbide tip tool, Centre lathe, Fluke IR Thermal Imager, Finite Element Analysis, Solid Modelling.

ACKNOWLEDGEMENT

The elation and gratification of the project will be incomplete without mentioning all the people who helped us to make it possible, whose gratitude and encouragement were invaluable to us.

Firstly we would like to thank GOD almighty, our supreme guide, for bestowing his blessings upon us in our entire endeavour.

We express our sincere thanks and gratitude to **Prof. Jyothi John**, Principal of this institution for providing the necessary facilities.

.We would like to express our sincere gratitude to **Mr. Sanchu S,** Project Guide, for his guidance and assistance in this thesis.

We express our sincere gratitude to **Mr. Manu M John**, Head of the Dept. for his support and guidance.

We also like to thank **Mr. Venkitaraj K P, Mr.Lasithan L G** and **Mr.Anoop A,** Project Coordinators, for their valuable words of advice.

We would also like to acknowledge with much appreciation the crucial role of the staff of Mechanical Laboratory, who gave the permission to use all required machinery and the necessary material to complete the experiment.

We also thankful to all students of our class for their support and suggestions.

TABLE OF CONTENTS

LIST OF TABLES

LIST OF FIGURES

ABBREVIATIONS

DOC	Depth of cut
EMF	Electro motive force
HSS	High speed steel
MRR	Material removal rate
ANOVA	Analysis of variance
2D	Two dimensional
3D	Three dimensional
APDL	Ansys parametric design language
DOF	Degrees of freedom

NOTATIONS

f	Feed rate
v	Cutting speed
d	Depth of cut
C	Correction Term
SS_{Total}	Total sum of squares
SS_{DOC}	Depth of cut sum of squares
SS_{Spd}	Speed sum of squares
$SS_{DOC*Spd}$	Speed*Depth of cut sum of squares
SS_{error}	Error sum of squares
$MS_{between}$	Mean of squares for between groups
MS_{error}	Mean of squares for error
r_i	Repeatability index
n	Number of sample size

CHAPTER 1
INTRODUCTION

1.1 GENERAL

A large amount of heat is generated during machining process as well as in different process where deformation of material occurs. The temperature that is generated at the surface of cutting tool when cutting tool comes in contact with the work piece is termed as cutting tool temperature. Heat is a parameter which strongly influences the tool performance during the operation. We know the power consumed in metal cutting is largely converted into heat. Temperature being developed during cutting it is of much concern as a result heat are mainly dependent on the contact between the tool and chip, the amount of cutting force and the friction between the tool and chip. Almost all the heat energy produced is transferred into the cutting tool and work piece material while a potion is dissipated through the chip. During machining the deformation process is highly concentrated in a very small zone and the temperatures generated in the deformation zone affect both the work piece and tool. Tool wear, tool life, work piece surface integrity, chip formation mechanism are strongly influenced at high cutting temperatures and contribute to the thermal deformation of the cutting tool, which is considered as the largest source of error in the machining process.

There has been a considerable amount of research devoted to develop analytical and numeric models in order to simulate metal cutting processes to predict the effects of machining variable such as speed, feed, depth of cut and also tool geometry on deformations of tool. Especially, numerical models are highly essential in predicting chip formation, computing forces, distributions of strain, strain rate, temperatures and stresses on the cutting edge and the machined work surface. Advanced process simulation techniques are necessary in order to study the influence of the tool edge geometry and cutting conditions on the surface integrity especially on the machining induced stresses. The objective is to analyze the temperature distribution on a tool of different materials at various machining parameters using analysis software ANSYS.

1.2 OBJECTIVES OF THE STUDY

Heat is a parameter which strongly influences the tool performance during the operation. So the machining can be improved by the knowledge of temperature distribution on the tool. Thus the main objectives of this project are as follows:

1. Study and comparison of temperature distribution on a single point cutting tool of different materials at various machining parameters.
2. Modelling and finite element analysis of single point cutting tool.
3. Comparison of experimental data with finite element analysis data for the tool.

There are different materials used for cutting tool such as HSS, cemented carbides, diamond etc. and the various machining parameters associated with the tool are cutting speed, feed and depth of cut. So in order to study the temperature distribution on the single point cutting tool we select different cutting tool materials and various machining parameters.

For carrying out the finite element analysis on the single point cutting tool Firstly we modelled the single point cutting tool using suitable modelling software. There are different modelling software are available such as AutoCAD, CATIA, SolidWorks, Pro/E etc. After modelling is done, this modelled single point cutting tool is imported into suitable finite analysis software such as ANSYS. So by providing suitable boundary conditions the finite element analysis of single point cutting tool is done. After finite element analysis, we compare the results obtained with experiment and finite element analysis data for the tool.

CHAPTER 2

LITERATURE SURVEY

2.1 THERMAL ASPECTS OF METAL MACHINING

Considerable heat is generated at the cutting edge of the tool due to friction between tool and work, and the plastic shearing of metal in the form of chips, when the tool is machining metal on a machine tool. The heat is evolved in three zones as shown in Figure 2.1.

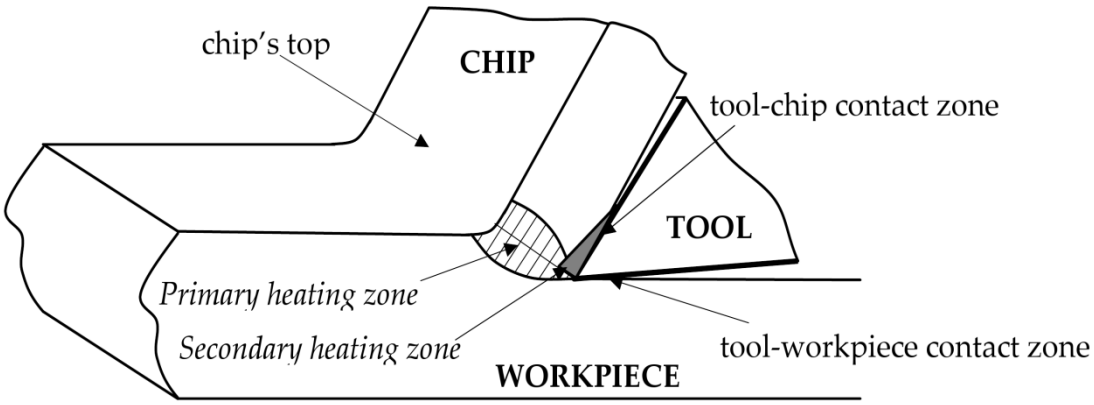

Figure 2.1 Evolution of heat at three zones

In shear zone, maximum heat is generated because of the plastic deformation of metal, and practically all of this heat is carried away by the chip as machining is rapid and continuous process. Avery minor portion of this heat (5-10%) is conducted to work piece. In friction zone, the heat is generated mainly due to friction between moving chip and tool face and partly due to secondary deformation of the built up edge. In work-tool contact zone, the heat is generated due to burnishing friction and the heat in this zone goes on increasing with time as the wear land on the tool develops and goes on increasing. It will be noted that each of these three zones leads to rise of temperature at the tool chip interface and it is found that the maximum temperature occurs slightly away from the cutting edge, and not at the cutting edge.

2.2 TOOL-CHIP INTERFACE TEMPERATURE

Measurement of tool temperature is important as the temperature distribution on the rake face of tool decides the tool wear and tool life. It can be measured by one of the following techniques:

2.2.1 THERMOCOUPLES

It is formed between tool and work piece. The hot end of tool and work piece and there Cold ends acts as thermocouple and emf proportional to temperature difference is produced. The work piece is insulated from the chuck and tailstock centre. The end of work piece is connected to a copper wire which dipped in mercury cup enables further connection serving as cold end. This point and connection from tool provide output for connection to a milli voltmeter. It is possible to obtain calibration curve between tool temperature and emf by laboratory methods.

2.2.2 EMBEDDED THERMOCOUPLES

The thermocouples are implanted in fine holes eroded in HSS tool from bottom face up to a fixed distance from the rake face, enabling measurement of temperature at several points along the rake face of tool.

2.2.3 INFRA-RED PHOTOGRAPHIC TECHNIQUE

This technique is based on taking photographs of the side face of tool-chip while cutting and comparing them with strips of known temperatures.

2.3 FACTORS AFFECTING CUTTING TEMPERATURE

The various factors which lead to maximum tool temperature affect the size of shear zone and chip tool contact length and thereby, the area over which heat is distributed. Shorter length of contact of chip with tool results in severe temperature rise. The various factors influencing cutting temperature are:

2.3.1 WORK PIECE AND TOOL MATERIAL

Tensile strength and hardness of work piece material have considerable influence on cutting temperature. If a material has high tensile strength and hardness, more energy is required for chip formation and more heat is generated. Materials with higher thermal conductivity produce lower temperature than tools with lower thermal conductivity.

2.3.2 CUTTING CONDITIONS

The cutting speed has predominant effect on the cutting temperature .Feed has little effect and depth of cut the least. The higher the cutting speed the faster the surface feet that the tool travels, the more heat will be generated by friction. The higher feed rate as well as depth of cut results in more material being removed, which result in higher friction.

2.3.3 CUTTING FLUID

At very high speeds the cutting fluid is not able to reach tool-chip interface and such cutting fluid does not affect the tool-chip interface temperature. The fluid is carried away by the outward flowing chip more rapidly than it could be forced between the tool and the chip.

2.3.4 TOOL GEOMETRY

Rake angle has only a slight influence on the temperature. Temperature variation of 20 °C only has been noted for rake angle changes from -10° to +30°. It increases with increase in approach angle and radius of tool.

2.4 REVIEW OF LITERATURE

The purpose of this chapter is to provide a review of past research efforts related to single-point cutting tool and finite element analysis. A review of other relevant research studies is also provided. The review is done to offer insight to how past research efforts have laid the groundwork for subsequent studies, including the present research effort. The review is detailed so that the present effort can be properly tailored to add to the present body of literature as well as to justify the scope and direction of the present effort.

B. Fnides, M. A. Yallese, H. Aouici [9] developed a work is to evaluate cutting pressures, resulting force and maximum temperature in hard turning of hot work steel AISI H11. This steel is hardened to 50 HRC, machined by a mixed ceramic tool (insert CC650 of chemical composition 70%Al_2O_3+30%TiC), free from tungsten on Cr-Mo-V basis, insensitive to temperature changes and having a high wear resistance. It is employed for the manufacture of highly stressed die casting moulds and inserts with high tool life expectancy, plastic moulds subject to high stress and forging dies. The tests of straight turning were carried out according to the method of planning experiments. The results made it possible to study the influence of cutting variables (feed rate, cutting speed and depth of cut) on cutting pressures, on resulting force and temperature in cutting zone. The effect of flank wear on cutting pressures is also studied. Mathematical model was deduced to express the influence degree of each cutting regime element on the maximum temperature. Thus, the ranges of best cutting conditions adapted, were given. Also this study confirms that in dry hard turning of this steel and for all cutting conditions tested, the major pressure is the radial pressure.

Shijun Zhang, Zhanqiang Liu [1] developed an analytical model with constant temperature at tool and chip interface of one-dimensional heat transfer in monolayer coated tools has been to investigate temperature distribution in metal cutting. The explicit form of temperature formulae were obtained by using the Laplace Transform technique and a Taylor series expansion. Calculations conducted for tools of three coatings (TiN, Tic and Al2O3) and two substrates (K10 and P10).

Rogério Fernandes Brito, Solidônio Rodrigues de Carvalho, Sandro Metrevelle Marcondes de Lima e Silva, João Roberto Ferreira [10] studies the heat influence in cutting tools considering the variation of the coating thickness and the heat flux. K10 and diamond tools substrate with TiN and Al2O3 coatings were used. The numerical methodology utilizes the ANSYS CFX software. Boundary conditions and constant thermo physical properties of the solids involved in the numerical analysis are known. To validate the proposed methodology an experiment is used.

L.B.Abhang and M. Hameedullah [2] developed first and second order mathematical models in terms of machining parameters by using the response surface methodology on the basis of the experimental results. The experiment was turning of EN-31 steel alloy with tungsten carbide inserts using a tool-work thermocouple technique. The results are analysed statistically and graphically. The metal cutting parameters considered are cutting speed, feed rate, depth of cut and tool nose radius.

J. E. Jam, V. N. Fard [3] determined the thermal contact conductance of the tool chip interface in the metal cutting process using an inverse procedure.An orthogonal cutting of the AISI 1045 steel is simulated by LS-DYNA finite element code. Tool chip interface average temperature is determined using thermo-mechanical coupled analysis of a two dimensional finite element model of the orthogonal cutting process under plane strain condition and compared with experimental measured data from literature during the inverse procedure. In thermo-mechanical coupled analysis friction condition in tool-chip interface is modelled using Coulomb's friction law together with the shear stress limits to describe the sliding and sticking condition on the tool rake face. The work piece material behaviour has been modelled using the Johnson Cook constitutive material model. Numerical simulation results of the orthogonal cutting process consisting of temperature in the tool-chip interface and cutting forces are shown and compared with experimental data reported in literature. Also, in this paper three dimensional thermal analysis of the cutting tool is performed.

Temperature distribution in three dimensional cutting tool model and thermal contact conductance of the tool-chip interface are also presented.

Yash R. Bhoyar, P. D. Kamble [4] studied the approaches for modelling the turning process for EN-24 type of steel. In this study, a Finite Element Analysis software Deform 3D is used to study the effects of cutting speed, feed rate, and type of alloy steel in temperature behaviour. The work-piece is modelled as Elastic-plastic material to take thermal, elastic, plastic effect. Work-piece is represented by a liner model with different length for each condition. Optical Infrared Pyrometer is used for the temperature measurement. This thermal device detect temperature of an object by reckoning the emitted, reflected and transmitted energy by means of optical sensors & detectors and show temperature reading on display panel.

Deepak Lathwal, Deepak Bhardwaj [5] studied three different rake angles in order to find out the variation in values of Vonmisses stress for the specified applied forces. In present study mesh is created in ANSYS and the boundary conditions are applied and the analysis is carried out for the applied constraints. The results calculated on software can be verified with experiments carried out with tool dynamometers for lathe tool. For future study the applied model can be used for multipoint cutting tools such as milling cutters, broaching tools etc.

Maheshwari N Patil, Shreepad Sarange [6] presented a methodology in order to determine tool forces and temperatures for use in finite element simulations of metal cutting processes. From the experimental set up, it is clearly observed that as depth of cut increases, the temperature generated in the tool at the tool tip also increases. It is also observed that, as the depth of cut increases, tool forces are also increases. It is main reason of tool failure. It is also observed that tool start vibrating at the depth of cut 2.5 mm. At this condition more heat is dissipated at the tool, due to which tool blunt. Experimental set up is made for force measurement during cutting using dynamometer and analyse the effect on the tool.

Meenu Sahu, Komesh Sahu [7] developed an optimization method of the cutting parameters (cutting speed, depth of cut and feed) in dry turning of AISI D2 steel to achieve minimum tool wear, low work piece surface temperature and maximum material removal rate (MRR). The experimental layout was designed based on the Taguchi's L9 (34) Orthogonal array technique and analysis of variance (ANOVA) was performed to identify the effect of the cutting parameters on the response variables. The results showed that depth of cut and cutting speed are the

most important parameter influencing the tool wear. The minimum tool wear was found at cutting speed of 150 m/min, depth of cut of 0.5 mm and feed of 0.25 mm/rev. Similarly low w/p surface temperature was obtained at cutting speed of 150 m/min, depth of cut of 0.5 mm and feed of 0.25 mm/rev. Whereas, at cutting speed of 250 m/min, depth of cut 1.00 mm and feed of 0.25 mm/rev, the maximum MRR was obtained. Thereafter, optimal range of tool wear, work piece surface temperature and MRR values were predicted. Finally, the relationship between factors and the performance measures were developed by using multiple regression analysis.

S. H. Rathod, Mohd. Razik [8] conducted three analyses using a High Speed Steel and of a Carbide Tip Tool at three different cutting speeds, in order to compare the experimental results produced. The experimental results reveal that the main factors responsible for increasing cutting temperature are cutting speed (v), feed rate (f), and depth of cut (d), respectively. **"**Fluke 62 max IR thermometer**"** is used for measuring temperature at tool-tip interface. Single point cutting tool has been solid modelled by using CAD Modeller Pro/E and FEA carried out by using ANSYS Workbench 14.5.By varying various parameters the effect of those on temperature are compared with the experimental results and FEA results. After comparison nearly 4% variation is found in between the results.

2.5 CONCLUSION OF LITERATURE SURVEY

The transient temperature distributions have shown that the thermo physical parameters of coating and substrate materials have huge influences on temperature distributions in monolayer coated tools. The analytical solution method has demonstrated that Al2O3 coating has more effective thermal barrier effect than the other two coating materials. The coating thickness also has some influence on temperature distributions in coated tools. Also work would be valuable for selecting coating materials in metal cutting process.

The TiN and Al2O3 coatings did not show satisfying results during a continuous cutting process. It showed a slight reduction in the heat flux for the 10 (μm) TiN and Al2O3 coatings.

The first order model that the cutting speed, feed rate and depth of cut are the most significantly influencing parameters for the chip-tool interface temperature followed by tool nose radius. Another quadratic model shows the variation of chip-

tool interface with major interaction effect between cutting speed and depth of cut (V*D) and second order (quadratic) effect of cutting speed (V2) appears to be highly significant. The results show that increase in cutting speed, feed rate and depth of cut increases the cutting temperature while increasing nose radius reduces the cutting temperature.

As we increase the rake angle then the value of Vonmisses stress goes on decreasing. The value of Vonmisses stress decrease for increase of rake angles of 7°, 9° and 11° respectively. From results it seems that reduction of resultant forces might cause increase in tool life but it cause decrease in tool life.

CHAPTER 3

METHODOLOGY

Mainly this project consists of two parts. They are Experiment and Finite Element Analysis.

3.1 DESIGN OF EXPERIMENT

In randomized complete block design, it is possible to reduce error variance by forming blocks such that the experimental units within the blocks are relatively more homogeneous with respect to the dependent variable of interest to the experimenter. The primary objective of creating the blocks is to eliminate from the experimental error the variation due to the differences between the blocks. The experimental units or the subjects correspond to plots and block comprises of k subjects that are fairly homogeneous with respect to a given variable. Here, each block will consist of k subjects matched on a given variable. Thus, the subjects within any block will be more homogeneous than the subjects that are selected at random. The objective of this local control is to create homogeneity within each of the r blocks and consequently heterogeneity between the blocks. The variation due to block differences is eliminated from the experimental error.

3.1.1 DESIGN OF EXPERIMENT FOR HSS TOOL

In our case, experimental results are the temperature formed at the cutting tool tip face when machining at different speed and depth of cut. Here we analyse the error using the temperatures obtained for HSS tool at a time 10 seconds after machining starts. The analysis carried out for a significance level of 0.01.The table of subjects of the design of experiment for HSS tool are summarized in Table 3.1

Speed (rpm)	Depth of Cut (mm)			Total Sum
	0.1	0.4	0.7	
150	34	70	115	937
	33	72	116	
	32	70	114	
	35	70	115	
	34	72	116	
420	73	96	148	1451
	72	94	146	
	73	95	145	
	71	94	146	
	72	95	145	
710	81	123	165	2144
	82	125	169	
	83	125	168	
	80	124	169	
	82	126	167	
Total Sum	1098	1565	1869	**4532**

Table 3.1 Table of subjects of the design of experiment for HSS tool

The computation procedures of the design of experiment for HSS tool are given below:

i. Correction Term, C = $(4532)^2/45$

= **456422.76**

ii. Total sum of squares, SS_{Total} = $(34)^2 + (33)^2 + \ldots\ldots + (167)^2 - C$

= 526056 – 456422.76

= **69633.24**

iii. DOC sum of squares, SS_{DOC} = $(1098)^2/15 + (1565)^2/15 + (1869)^2/15 - C$

= 476532.67 – 456422.76

= **20109.91**

iv. Speed sum of squares, SS_{Spd} = $(937)^2/15 + (1451)^2/15 + (2144)^2/15 - C$

= 505340.4 – 456422.76

= **48917.64**

v. Speed*DOC sum of squares, $SS_{DOC*Spd}$ = $(168)^2/5 + (361)^2/5 + \ldots..+ (838)^2/5 - C - SS_{DOC} - SS_{Spd}$

= 526010 - 456422.76 - 20109.91-48917.64

= **559.64**

vi. Error sum of squares, SS_{error} = SS_{Total} - (SS_{DOC} -SS_{Spd}- $SS_{DOC*Spd}$)

= 69633.24- (20109.91+48917.64+ 559.69)

= **46**

3.1.2 DESIGN OF EXPERIMENT FOR CARBIDE TOOL

Similarly here also we analyse the error using the temperatures obtained for Carbide tool at a time 10 seconds after machining starts. The analysis carried out for a significance level of 0.01.The table of subjects are summarized in table 3.2

Speed (rpm)	Depth of Cut (mm)			Total Sum
	0.1	0.4	0.7	
150	37	71	118	1006
	39	71	119	
	40	72	120	
	39	73	119	
	38	72	119	
420	75	102	153	1509
	76	102	153	
	77	103	154	
	75	104	153	
	76	104	155	
710	87	127	176	2239
	88	128	175	
	86	127	176	
	86	128	174	
	87	127	175	
Total Sum	1147	1662	1945	**4754**

Table 3.2 Table of subjects of the design of experiment for Carbide tool

The computation procedures of the design of experiment for Carbide tool are given below:

i. Correction Term, C = $(4754)^2/45$

= **502233.69**

ii. Total sum of squares, SS_{Total} = $(37)^2 + (39)^2$+…… + $(175)^2$ - C

= 575588N– 502233.69

= **73354.31**

iii. DOC sum of squares, SS_{DOC} = $(1147)^2/15 + (1662)^2/15 + (1945)^2/15$ - C

= 524058.53 – 502233.69

= **21824.84**

iv. Speed sum of squares, SS_{Spd} = $(1006)^2/15 + (1509)^2/15 + (2239)^2/15 - C$

= 553487.52 – 502233.69

= **51248.84**

v. Speed*DOC sum of squares, $SS_{DOC*Spd}$ = $(193)^2/5 + (359)^2/5 + \ldots..+ (876)^2/5 - C - SS_{DOC} - SS_{Spd}$

= 575560.4 – 502233.69 – 21824.84 – 51248.84

= **253.03**

vi. Error sum of squares, SS_{error} = $SS_{Total} - (SS_{DOC} - SS_{Spd} - SS_{DOC*Spd})$

= 73354.31- (51248.84+21824.84+ 253.03)

= **27.6**

3.1.3 REPEATABILITY TEST

The repeatability index (r_i) can be used to assess precision i.e. whether an observer makes consistent measurements and whether a trial varies.

$$r_i = (MS_{between} - MS_{error}) / (MS_{between} + (n-1)\, MS_{error})$$

Informal terms to describe the measure of repeatability r_i, from Martin and Bateson (1986) is summarized in table 3.3

Index of repeatability (r_i)	Term
$r_i < 0.2$	Slight repeatability
$0.2 < r_i < 0.4$	Low repeatability
$0.4 < r_i < 0.7$	Moderate repeatability
$0.7 < r_i < 0.9$	High repeatability
$r_i > 0.9$	Very high repeatability

Table 3.3 Informal terms to describe the measure of repeatability

3.1.4 EXPERIMENTAL SETUP AND CONDITIONS

The experiment was conducted under dry conditions on a three jaw centre lathe. Lathe removes undesired material from a rotating work piece in the form of chips with the help of tool which is traversed across the work and can be fed deep in

work. A hole was drilled on the face of work piece to allow it to be supported at the tailstock (Figure 3.1).

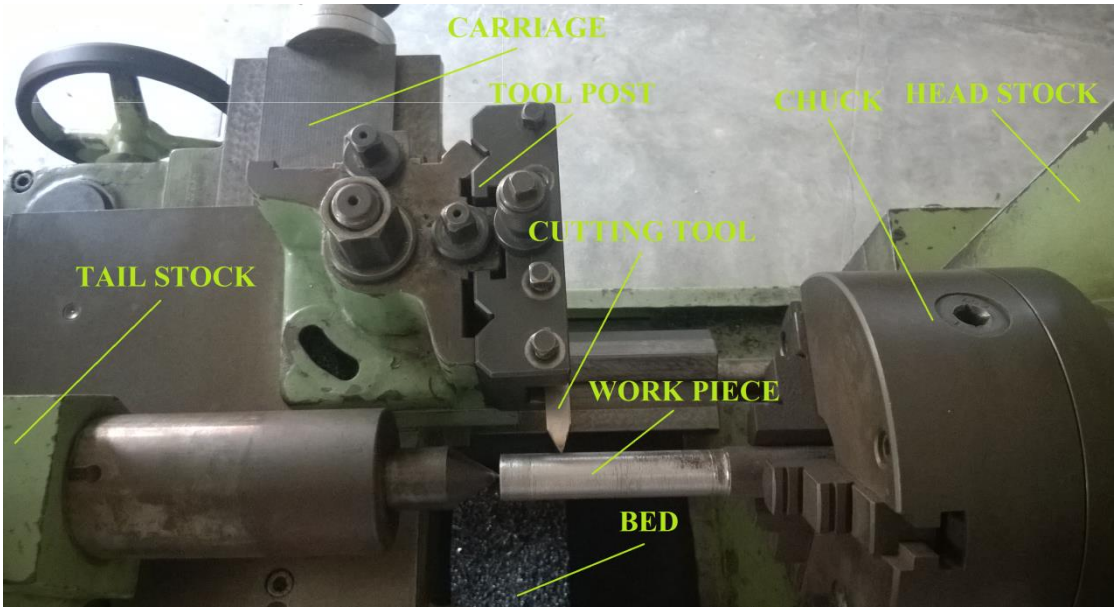

Figure 3.1 Experimental setup

The work piece used as cylindrical rod of Mild Steel (Ø23*63.7 mm). The cutting tool used as High Speed Steel and Carbide Tip Tool (13*101.98 mm). The machining is carried out at different speed and depth of cut. Feed may be kept as constant. The settings of the main machining parameters are summarized in Table 3.4.

Parameters	**Value**
Feed (mm/rev)	0.52
Speed (rpm)	150, 420, 710
Depth of cut (mm)	0.1, 0.4, 0.7

Table 3.4 Main machining parameters of the experiment

We know that maximum temperature is on the tool chip interface during machining. So for measuring this temperature we use a Thermal imager, a non-contact temperature measurement device. Thermal imagers detect the infrared energy emitted, transmitted or reflected by all materials (at temperatures above absolute zero) and converts the energy factor into a temperature reading or thermo gram. A thermo gram is the thermal image displayed by the camera of the object which is emitting,

transmitting or reflecting the infrared energy. Here Fluke TI32 IR Thermal Imager (Range -20 °C to +600 °C) is used for measuring the temperature on the cutting tool while machining (Figure 3.2). Stop watch is used for measuring the time for machining.

Figure 3.2 Fluke TI32 IR Thermal Imager

3.2 FINITE ELEMENT ANALYSIS OF TOOL

Finite element analysis of single point cutting tool is carried out by using ANSYS, a powerful general purpose finite element analysis package. Ansys is a finite element analysis package to numerically solve a wide variety of mechanical, structural and non-structural problems. These problems include static/dynamic structural analysis (both linear and non-linear), heat transfer and fluid problems as well as acoustic and electromagnetic problems.

In this project we carried out thermal analysis of a single point cutting tool using Ansys. Thermal analysis is used for determining the temperature distribution and quantities such as thermal distribution, amount of heat loss or gain, thermal gradient, thermal fluxes etc.

The problem analysing here is basically a multiphysics coupling (structural - thermal). Usually, physics coupling is ignored or simplified. Simulation engineers are usually using single-physics. Because coupled analyses are more computationally intensive. However, coupled analyses provide more realistic results. ANSYS Workbench is designed to make it easier to simulate multiphysics coupling.

Regarding coupling methodology, multiphysics coupling can be classified as two. They are sequential coupling and direct coupling. In sequential coupling, coupling is considered in one direction only whereas in direct coupling, coupling is considered in both directions. 1-way thermal to structural coupling can be easily defined in Workbench. However, 1-way structural to thermal coupling is not possible in ANSYS. Direct coupling is available in ANSYS, but not in the Workbench interface. To represent direct coupling, APDL commands should be used. User must select coupled-field elements. 1-way structural to thermal coupling is usually represented by direct coupling as well. It's easier than export the deformed mesh and results from the structural analysis to the thermal analysis.

ANSYS includes the coupled elements such as SOLID5, PLANE13, SOLID98, PLANE223, SOLID226, SOLID227 etc.

The analysis procedure consists of three phases such as pre-processing, solution and post processing. The Pre-processing phase consists of defining geometry, material, mesh, load and boundary conditions. The solution phase consists of defining analysis settings and convergence. The post processing phase consists of obtaining results.

3.2.1 MODELLING OF TOOL

The single point cutting tool has been solid modelled by using SOLIDWORKS, a solid modelling computer aided design software. Solidworks is a solid modeller, and utilizes parametric feature-based approach to create models and assemblies. Parameters refer to constraints whose values determine the shape of or geometry of the model or assembly. Parameters can be either numeric parameter, such as tangent, parallel, concentric, horizontal or vertical etc. numeric parameters can be associated with each other through the use of relations.

The main dimensions of the tool and work piece is summarized below in Table 3.5

	Cutting Tool	Work piece
Material	High Speed Steel Tungsten carbide	Mild Steel
Cross-section	13*101.98 mm Side and end cutting edge angles: 30° End relief angle: 20°	Ø23*63.7 mm

Table 3.5 Main dimensions of the tool and work piece

3.2.1.1 MODELLING OF HSS TOOL

The single point cutting tool (HSS) has been solid modelled by using SOLIDWORKS. The 3D and 2D views are shown in below (Figure 3.3 and 3.4).

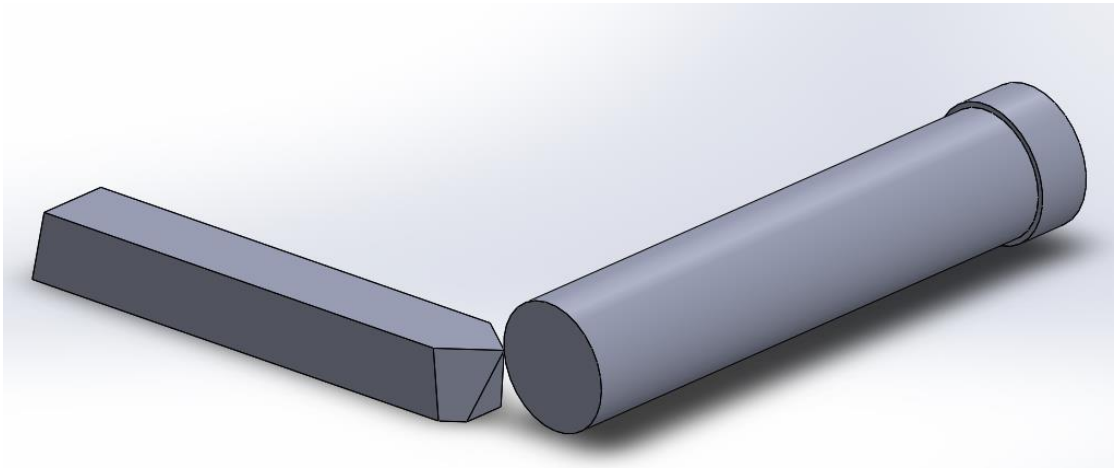

Figure 3.3 3D view of HSS model

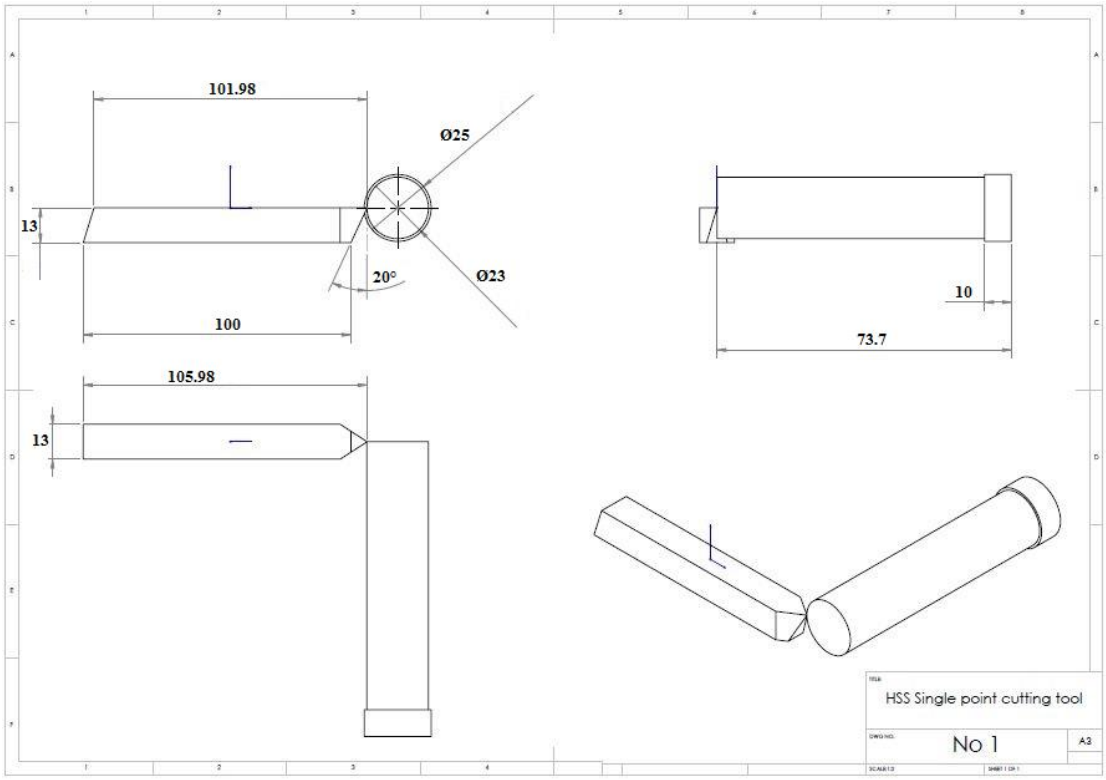

Figure 3.4 2D view of HSS model

3.2.1.2 MODELLING OF CARBIDE TOOL

The single point cutting tool (Tungsten Carbide) has been solid modelled by using SOLIDWORKS. The 3D and 2D views are shown in below (Figure 3.5 and 3.6).

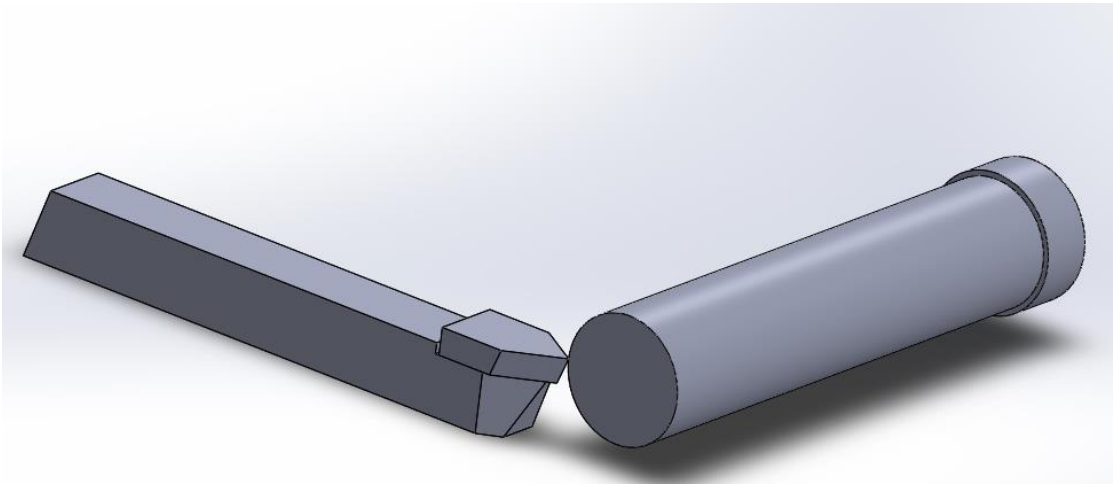

Figure 3.5 3D view of Carbide model

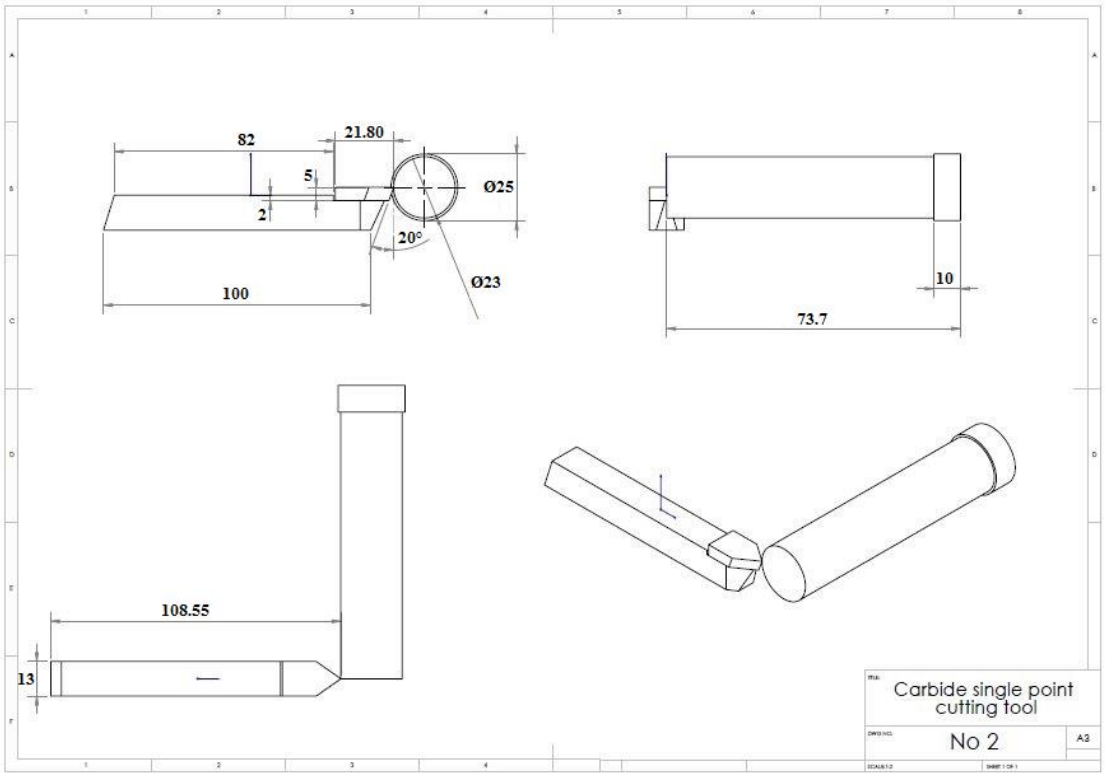

Figure 3.6 2D view of Carbide model

3.2.2 FINITE ELEMENT ANALYSIS OF HSS TOOL

3.2.2.1 GEOMETRY

The geometry is modelled using 'SOLIDWORKS-2013'and then it is imported into 'ANSYS WORKBENCH'

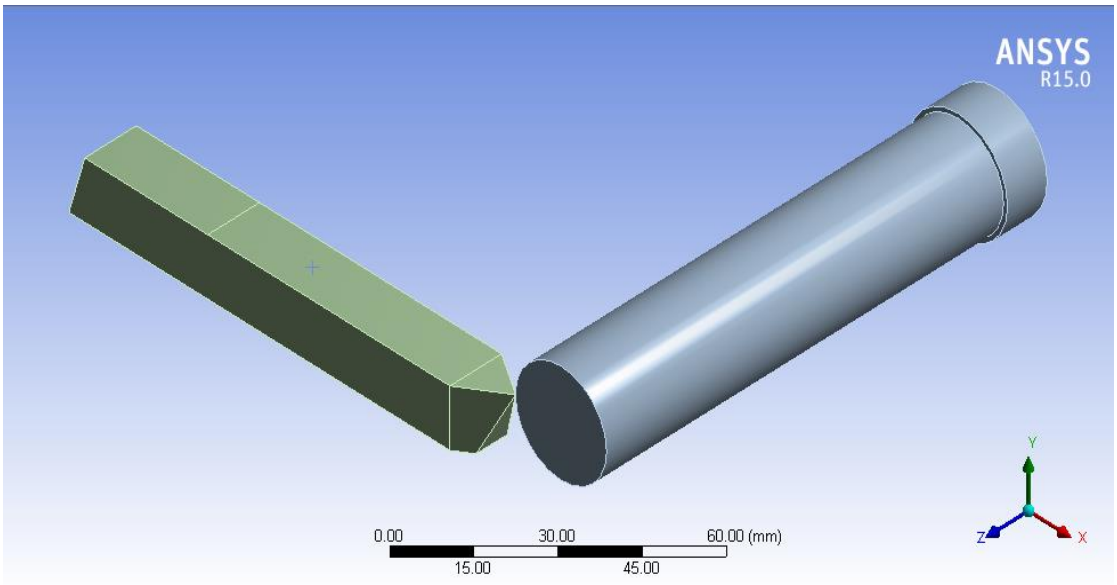

Figure 3.7 Geometry of HSS tool

3.2.2.2 MATERIAL

The cutting material used is T15 super high speed steel. The temperature dependent properties of tool are summarised below in Table 3.6 and the other properties are also given below.

Sl No	Temperature (°C)	Density (kg/m^3)	Thermal Conductivity(w/mK)	Specific Heat(J/kgK)
1	0	8190	19	418.68
2	50	8186	20	420
3	75	8183	22	425.36
4	100	8179	23	430.45
5	120	8177	25	436.25
6	175	8172	26	442.57
7	200	8168	28	445.68
8	220	8162	30	448.35

Table 3.6 Properties of T15 super high speed steel

Coefficient of thermal expansion: $1.01*10^{-5}$ °C^{-1} (Ref temp: 22 °C)

Young's modulus: $2.07*10^5$ Mpa

Poisson's ratio: 0.25

The work piece material used is mild steel. The various properties of mild steel are given below,

Density: 7850 kg/m^3

Coefficient of thermal expansion: $1.2*10^{-5}$ °C^{-1} (Ref temp:20 °C)

Young's modulus: $2*10^{11}$ Pa

Poisson's ratio: 0.3

Thermal conductivity: 60.5 w/mK

Specific heat: 434 J/kgK

Next step is, An APDL command is used to change element type. Element must be chosen accordingly to mesh geometry. Here 'Brick 20 node SOLID 226' is used as work piece element and 'Tetra 10 node SOLID227' is used as cutting tool element.

The SOLID226 element has twenty nodes with up to five degrees of freedom per node. Structural capabilities include elasticity, plasticity, viscoelasticity, viscoplasticity, creep, large strain, large deflection, stress stiffening effects, and prestress effects. Thermoelectric capabilities include Seebeck, Peltier, and Thomson effects, as well as Joule heating. In addition to thermal expansion, structural-thermal

capabilities include the piezocaloric effect in dynamic analyses. The Coriolis Effect is available for analyses with structural degrees of freedom. The thermoplastic effect is available for analyses with structural and thermal degrees of freedom. The diffusion expansion effect is available for analyses with structural and diffusion degrees of freedom.

The SOLID227 element has twenty nodes with up to five degrees of freedom per node. Structural capabilities include elasticity, plasticity, viscoelasticity, viscoplasticity, creep, large strain, large deflection, stress stiffening effects, and prestress effects. Thermoelectric capabilities include Seebeck, Peltier, and Thomson effects, as well as Joule heating. In addition to thermal expansion, structural-thermal capabilities include the piezocaloric effect in dynamic analyses. The Coriolis Effect is available for analyses with structural degrees of freedom. The thermoplastic effect is available for analyses with structural and thermal degrees of freedom. The diffusion expansion effect is available for analyses with structural and diffusion degrees of freedom.

The APDL command used for changing the element type is given below.

ET, matid, SOLID 226: This changes element type to SOLID226.

KEYOPT, mat id, 1, 11: This defines Thermal-Structural behaviour.

ET, matid, SOLID227: This changes element type to SOLID227.

KEYOPT, mat id, 1, 11: This defines Thermal-Structural behaviour.

3.2.2.3 MESHING

The method used for meshing the cutting tool is ‘Hex dominant method’giving a body sizing of 1.5 mm and for work piece is ‘Multi zone method’ giving a body sizing of 2.5 mm.The meshed geometry is given in Figure 3.8.

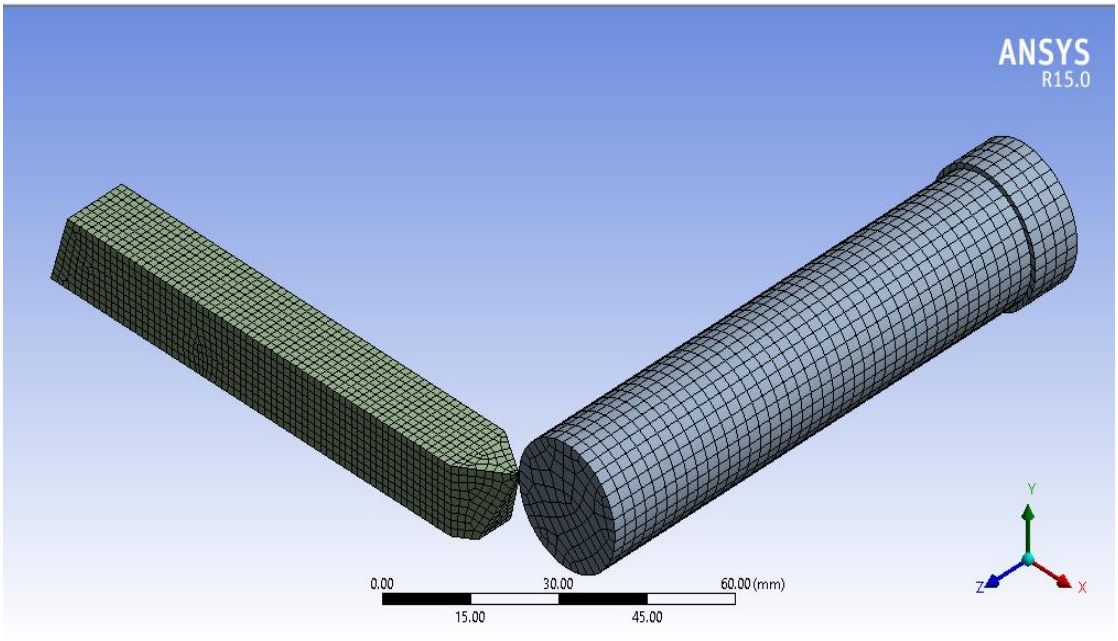

Figure 3.8 Meshed geometry of HSS tool

For mesh convergence study, different mesh element sizes are provided for cutting tool as well work piece. The objective of this study is to reduce the error as well as the computational time. The summarized study is given below in Table 3.7.

Work piece element size [mm]	Cutting Tool element size [mm]	Number of nodes	Number of Elements	Max FEA Temp [°C]	Max Expt Temp [°C]	%error	Computational Time [Hrs]
4	3	13231	2971	80.2	**67.6**	15.71	74.6
3.5	2.5	18678	3975	78.9		14.32	102.2
3	2	25345	5340	72.1		6.241	105.65
2.5	**1.5**	**49197**	**11059**	**69**		**2.03**	**115.94**
2	1	144399	36793	68.8		1.744	140.45
1.5	0.5	725465	183714	68.7		1.601	163.2

Table 3.7Mesh convergence study

3.2.2.4 LOAD AND BOUNDARY CONDITIONS

Structural loads and boundary conditions are applied as usual. Here we have four conditions.

1.Cylindrical support for work piece

2.Longitudinal displacement of tool (63.7 mm)

3.Tangential displacement of tool (0.1 mm, 0.4 mm, 0.7 mm)

4.Speed of rotation of work piece (150 rpm, 420 rpm, 710 rpm)

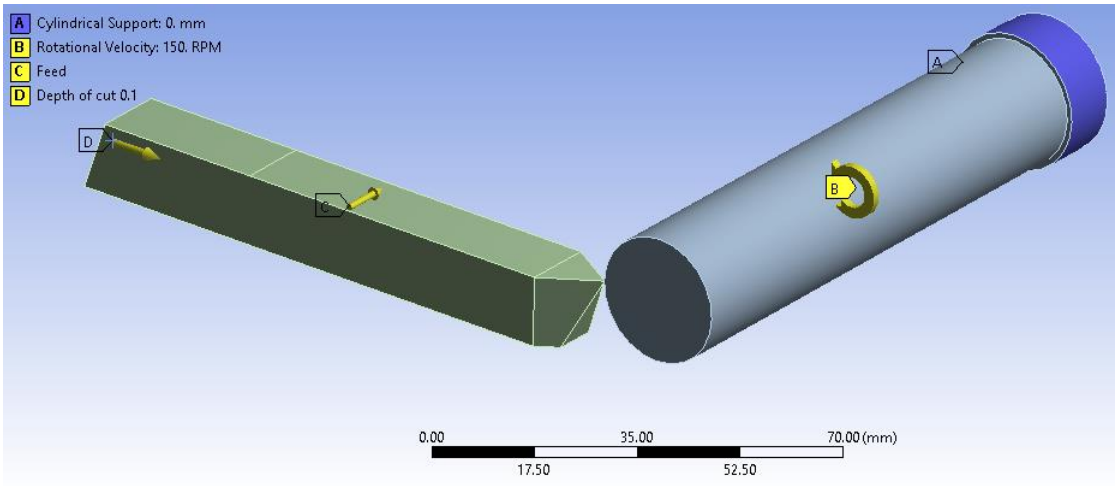

Figure 3.9 Load and boundary conditions for HSS tool

Here the model is defined as frictional model. That is heat is generated due to contacting friction when machining. So we define a contact element and target element. In this case, cutting tool is contact element (CONTA175) and work piece is the target element (TARGE170) and a node to surface contact is obtained. The coefficient of friction is given as 0.5 and contact behaviour is asymmetric.

CONTA175 may be used to represent contact and sliding between two surfaces (or between a node and a surface, or between a line and a surface) in 2-D or 3-D. The element is applicable to 2-D or 3-D structural and coupled field contact analyses. This element is located on the surfaces of solid, beam, and shell elements. 3D solid and shell elements with midside nodes are supported for bonded and no separation contact. For other contact types, lower order solid and shell elements are recommended.

Contact occurs when the element surface penetrates one of the target segment elements (TARGE169, TARGE170) on a specified target surface. Coulomb friction, shear stress friction, user-defined friction with the USERFRIC subroutine, and user-defined contact interaction with the USERINTER subroutine are allowed. This element also allows separation of bonded contact to simulate interface delamination.

The below APDL commands are for changing the behaviours of contact elements.

KEYOPT, cid, 1, 1: This includes displacement and temperature degrees of freedom

KEYOPT, cid, 5, 3: This close gap or reduce penetration.

KEYOPT, cid, 9, 1: Exclude both initial penetration and gap.

KEYOPT, cid, 10, 2: Contact stiffness update on each iteration based.

The below APDL commands are for modifying the real constant sets. **RMODIF, cid, 9, 500e6**: This changes maximum frictional stress in N/m^2

RMODIF, cid, 14, 1e4: This changes thermal contact conductance between tool and work piece in w/m^2 °C

RMODIF, cid, 15, 1: This includes a real constant FHTG , the fraction of frictional dissipated energy converted into heat.

RMODIF, cid, 18, 0.95: This gives fraction of frictional dissipated energy converted into heat.

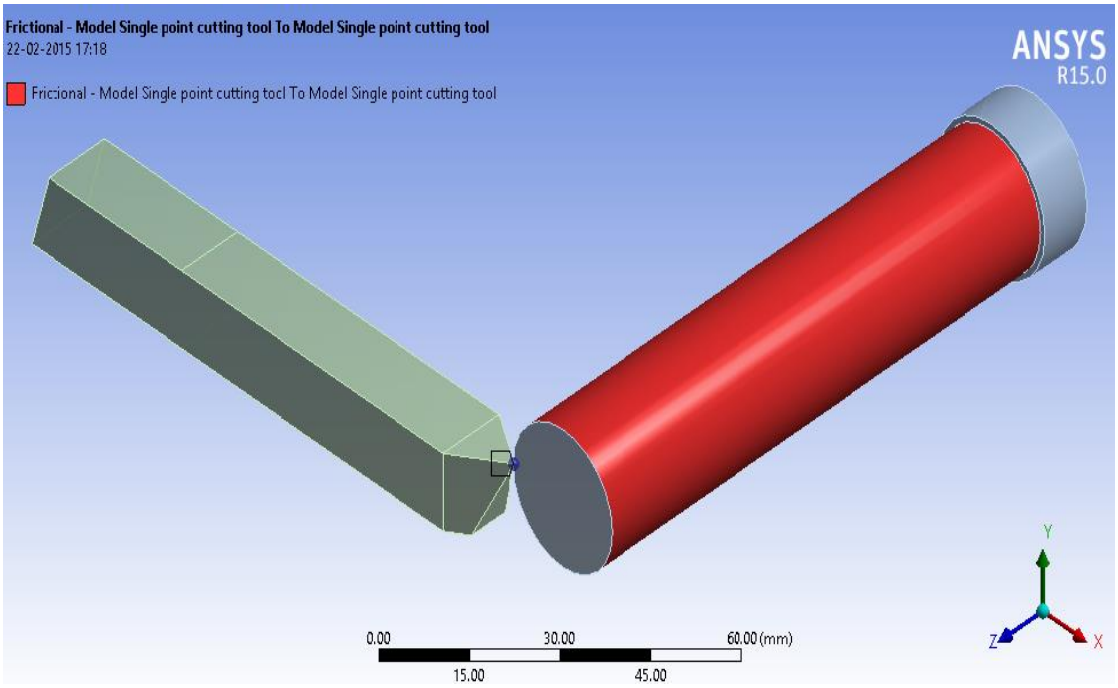

Figure 3.10 Frictional model of HSS tool

3.2.2.5 ANALYSIS SETTINGS

For time step controls, program controlled (automatic) time step are used. The step end times are 49 sec, 17.5 sec and 10.0 sec. The initial time step may be given as 0.49 sec, 0.175 sec and 0.10 sec. The ranges for time step are given as,

Minimum time step: $4.9*10^{-2}$ sec, $1.75*10^{-2}$ sec, $1.0*10^{-2}$ sec.

Maximum time step: 4.9 sec, 1.75 sec, 1.0 sec.

For non-linear control, Unsymmetric Newton Raphson method is used.

The below APDL commands are for setting thermal boundary conditions and analysis settings.

/SOLU: To enter into solution stage

TREF, 22: Setting reference temperature to 22 °C.

SF, conv-face, CONV, 200, 22: To give convection condition with its film coefficient and bulk temperature.

ALLSEL: Select all entities.

TRNOPT, full: Switching transient analysis option to full method which is more accurate.

3.2.2.6 SOLUTION

Analysis can be solved as usual. Thermal results can be plotted with the User-defined Result. For that select solution and click Worksheet (Figure 3.11).

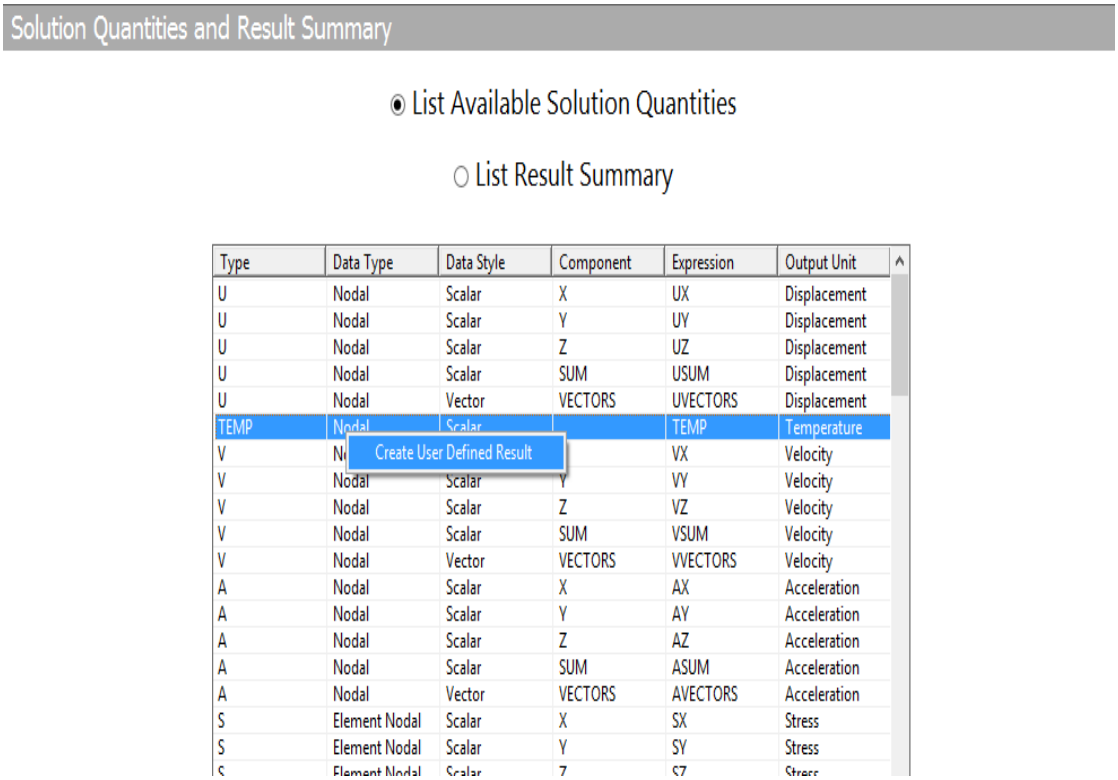

Figure 3.11 Selection of solution quantities for HSS tool

3.2.3 FINITE ELEMENT ANALYSIS OF CARBIDE TOOL

3.2.3.1 GEOMETRY

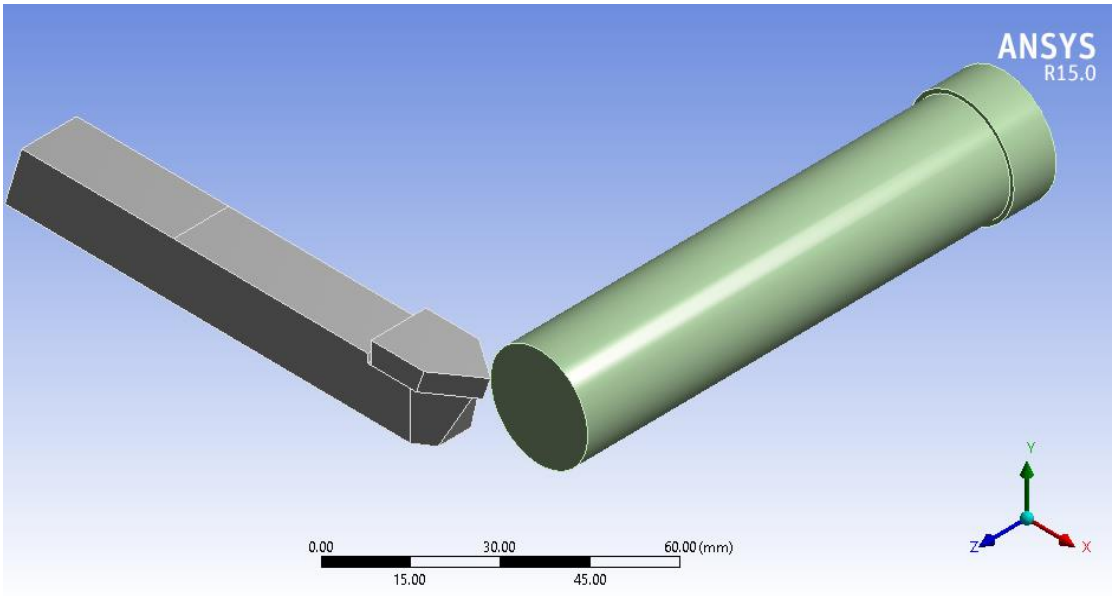

Figure 3.12 Geometry of Carbide tool

3.2.3.2 MATERIAL

The cutting tool tip material used is C20 Tungsten Carbide. The temperature dependent properties of tool are summarised below in Table 3.8 and the other properties are also given below.

Sl No	Temperature (C)	Density (g/cm^3)	Thermal Conductivity(w/mK)	Specific Heat(J/kgK)
1	0	14.90	84	210
2	50	14.70	84.5	212.3
3	75	14.67	85	213.5
4	100	14.62	85.5	214
5	150	14.58	87	215.8
6	175	14.55	87.4	216.8
7	200	14.45	87.8	217.3
8	230	14.40	88.2	218

. Table 3.8 Properties of C20 Tungsten Carbide

Coefficient of thermal expansion: $5.2*10^{-6}$ °C^{-1} (Ref temp: 25 °C)

Young's modulus: $6.1*10^5$ Mpa

Poisson's ratio: 0.25

The shank material used for the tool is medium carbon steel. The various properties of medium carbon steel are given below,

Density: 7870 kg/m^3

Coefficient of thermal expansion: $1.3*10^{-5}$ C^{-1} (Ref temp: 25 °C)

Young's modulus: $2*10^{5}$ Mpa

Poisson's ratio: 0.29

Thermal conductivity: 60.5 W/mK

Specific heat: 434 J/kg/K

The work piece material used is mild steel. The various properties of mild steel are given below,

Density: 7850 kg/m^3

Coefficient of thermal expansion: $1.2*10^{-5}$ $°C^{-1}$ (Ref temp: 20 °C)

Young's modulus: $2*10^{11}$ Pa

Poisson's ratio: 0.3

Thermal conductivity: 60.5 w/mK

Specific heat: 434 J/kgK

Next step is, An APDL command is used to change element type. Element must be chosen accordingly to mesh geometry. Here 'Brick 20 node SOLID 226' is used as work piece element and 'Tetra 10 node SOLID227' is used as cutting tool element.

The APDL command used for changing the element type is given below.

ET, matid, SOLID 226: This changes element type to SOLID226.

KEYOPT, mat id, 1, 11: This defines Thermal-Structural behaviour.

ET, matid, SOLID227: This changes element type to SOLID227.

KEYOPT, mat id, 1, 11: This defines Thermal-Structural behaviour.

3.2.3.3 MESHING

The method used for meshing the cutting tool is 'Hex dominant method'giving a body sizing of 1.5 mm and for work piece is 'Multi zone method' giving a body sizing of 2.5 mm.The meshed geometry is given in Figure 3.13

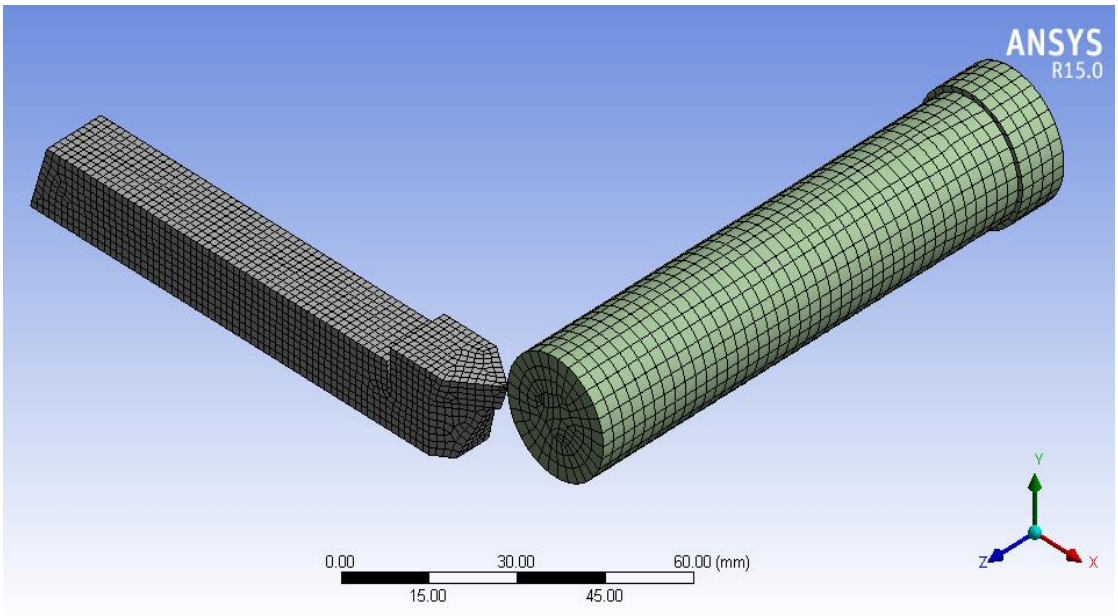

Figure 3.13 Meshed geometry of Carbide tool

3.2.3.4 LOAD AND BOUNDARY CONDITIONS

Structural loads and boundary conditions are applied as usual. Here we have four conditions.

1.Cylindrical support for work piece

2.Longitudinal displacement of tool (63.7 mm)

3.Tangential displacement of tool (0.1 mm, 0.4 mm, 0.7 mm)

4.Speed of rotation of work piece (150 rpm, 420 rpm, 710 rpm)

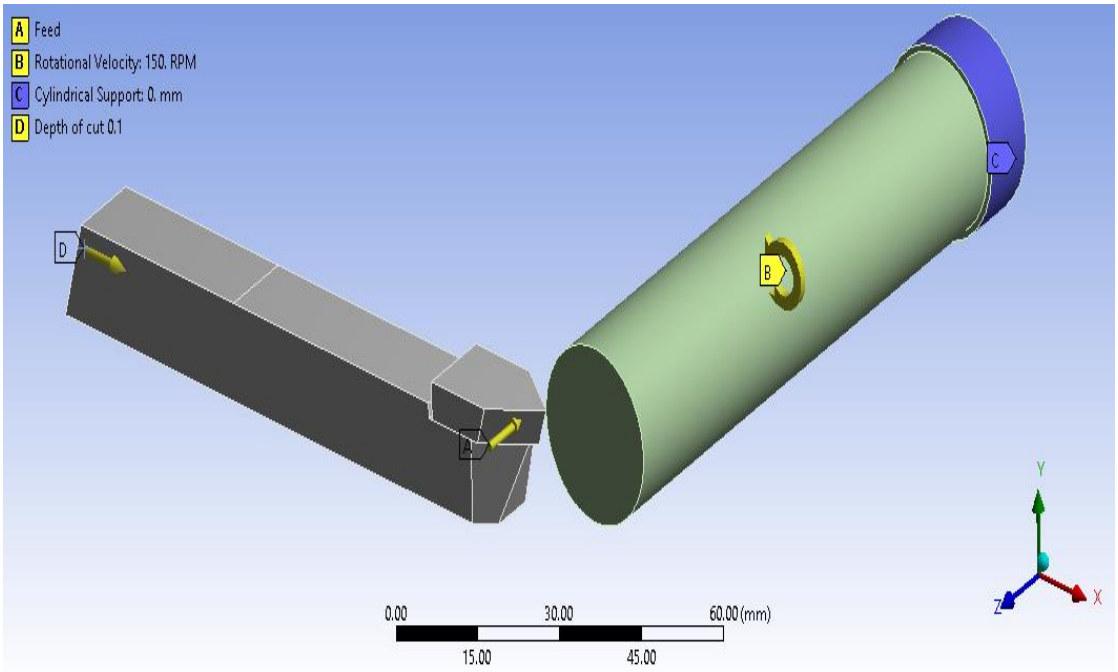

Figure 3.14 Load and boundary conditions for Carbide tool

Here the model is defined as frictional model. That is heat is generated due to contacting friction when machining. So we define a contact element and target element. In this case, cutting tool is contact element (CONTA175) and work piece is the target element (TARGE170) and a node to surface contact is obtained. The coefficient of friction is given as 0.3 and contact behaviour is asymmetric.

The below APDL commands are for changing the behaviours of contact elements.

KEYOPT, cid, 1, 1: This includes displacement and temperature degrees of freedom

KEYOPT, cid, 5, 3: This close gap or reduce penetration.

KEYOPT, cid, 9, 1: Exclude both initial penetration and gap.

KEYOPT, cid, 10, 2: Contact stiffness update on each iteration based.

The below APDL commands are for modifying the real constant sets.

RMODIF, cid, 9, 500e6: This changes maximum frictional stress in N/m^2

RMODIF, cid, 14, 1e4: This changes thermal contact conductance between tool and work piece in w/m^2 °C

RMODIF, cid, 15, 1: This includes a real constant FHTG , the fraction of frictional dissipated energy converted into heat.

RMODIF, cid, 18, 0.95: This gives fraction of frictional dissipated energy converted into heat.

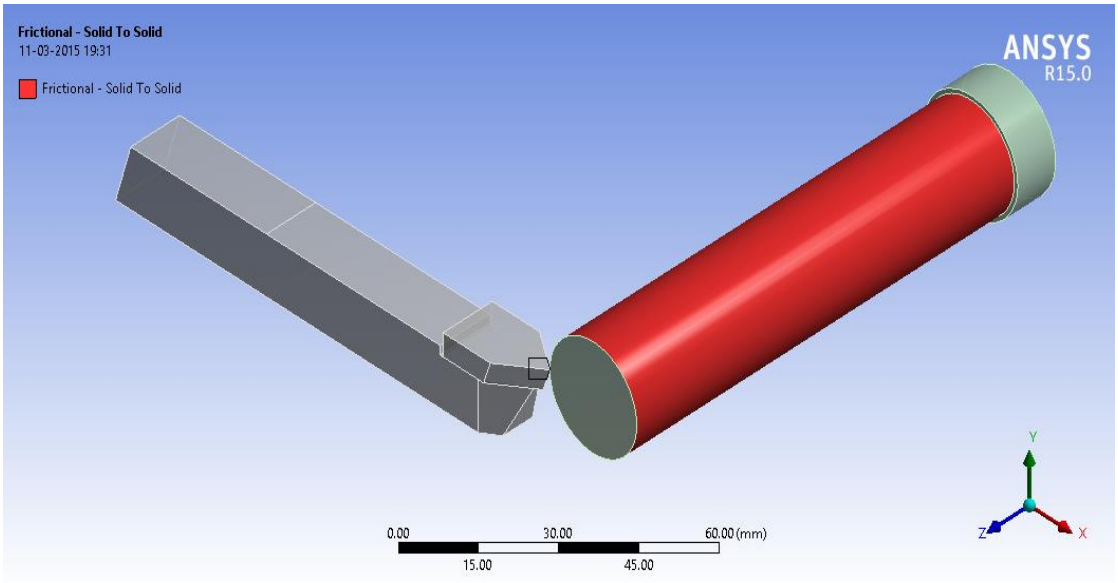

Figure 3.15 Frictional model of Carbide tool

3.2.3.5 ANALYSIS SETTINGS

For time step controls, program controlled (automatic) time step are used. The step end times are 49 sec, 17.5 sec and 10.0 sec. The initial time step may be given as 0.49 sec, 0.175 sec and 0.10 sec. The ranges for time step are given as,

Minimum time step: $4.9*10^{-2}$ sec, $1.75*10^{-2}$ sec, $1.0*10^{-2}$ sec.

Maximum time step: 4.9 sec, 1.75 sec, 1.0 sec.

For non-linear control, Unsymmetric Newton Raphson method is used.

The below APDL commands are for setting thermal boundary conditions and analysis settings.

/SOLU: To enter into solution stage

TREF, 22: Setting reference temperature to 22 °C.

SF, conv-face, CONV, 200, 22: To give convection condition with its film coefficient and bulk temperature.

ALLSEL: Select all entities.

TRNOPT, full: Switching transient analysis option to full method which is more accurate.

3.2.3.6 SOLUTION

Analysis can be solved as usual. Thermal results can be plotted with the User-defined Result. For that select solution and click Worksheet (Figure 3.16).

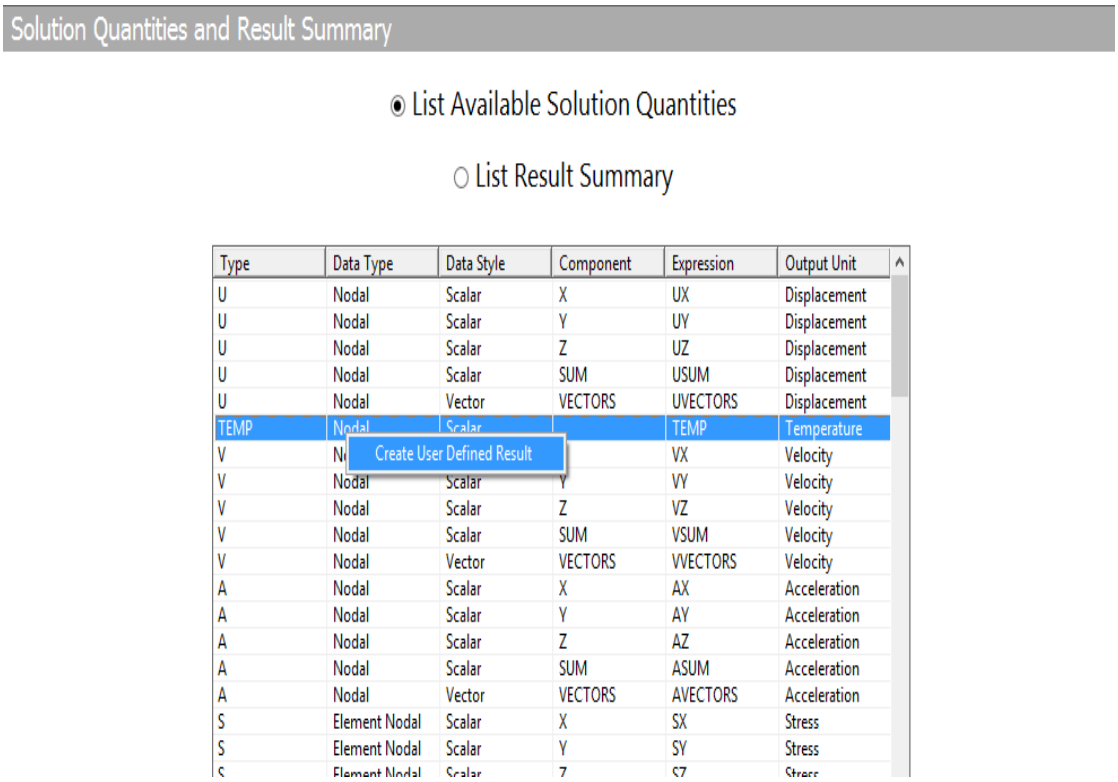

Figure 3.16 Selection of solution quantities for Carbide tool

CHAPTER 4

RESULTS AND DISCUSSION

4.1 ANALYSIS OF VARIANCE OF THE DESIGN OF EXPERIMENT FOR HSS TOOL

The analysis of variance of the design of experiment for HSS tool are summarized in table 4.1

Source of variation	Sum of squares	DOF	Mean of squares	F_{Static}	$F_{Critical}$	P	% C
Speed	48917.64	2	244458.82	19108.45	5.25	< 0.01	70.25
DOC	20109.91	2	10054.96	7855.44	5.25	< 0.01	28.88
Speed*DOC	559.64	4	139.92	109.31	3.89	< 0.01	0.80
Error	46	36	1.28				0.066
Total Sum	69633.24	44					100

Table 4.1 Analysis of variance of the design of experiment for HSS tool

From the ANOVA table, it is clear that speed is the most significant parameter followed by depth of cut. However the interaction of speed*depth of cut has least effect.

4.2 REPEATABILITY TEST FOR HSS TOOL

The measure repeatability for HSS tool is summarized in Table 4.2.

Source of variation	Mean of squares	Index of repeatability	Term
Speed	24458.82	0.9997	Very high repeatability
DOC	10054.96	0.9993	Very high repeatability
Speed*DOC	139.92	0.955	Very high repeatability
Error	1.28		

Table 4.2 Measure of repeatability for HSS tool

4.3 ANALYSIS OF VARIANCE OF THE DESIGN OF EXPERIMENT FOR CARBIDE TOOL

The analysis of variance of the design of experiment for Carbide tool are summarized in table 4.3

Source of variation	Sum of squares	DOF	Mean of squares	F_{Static}	$F_{Critical}$	P	% C
Speed	51248.84	2	25624.42	33278.47	5.25	< 0.01	69.86
DOC	21824.84	2	10912.42	14171.97	5.25	< 0.01	29.75
Speed*DOC	253.03	4	63.26	82.16	3.89	< 0.01	0.35
Error	27.6	36	0.77				0.038
Total Sum	73354.31	44					100

Table 4.3 Analysis of variance of the design of experiment for Carbide tool

From the ANOVA table, it is clear that speed is the most significant parameter followed by depth of cut. However the interaction of speed*depth of cut has least effect.

4.4 REPEATABILITY TEST FOR CARBIDE TOOL

The measure repeatability for Carbide tool is summarized in Table 4.4.

Source of variation	Mean of squares	Index of repeatability	Term
Speed	25624.42	0.9998	Very high repeatability
DOC	10917.42	0.9996	Very high repeatability
Speed*DOC	63.26	0.942	Very high repeatability
Error	0.77		

Table 4.4 Measure of repeatability for Carbide tool

4.5 EXPERIMENTAL AND FINITE ELEMENT ANALYSIS RESULTS FOR HSS TOOL

The temperatures obtained for high speed steel tool at various speed and depth of cut through experiment and FEA are summarized in Tables and graphs given below.

4.5.1 TEMPERATURE OBTAINED AT SPEED: 150 rpm, DOC: 0.1 mm

Sl No	Time [sec]	Max Temp [°C]
1	0	29.4
2	10	33.6
3	20	37.8
4	30	48.6
5	40	58.2
6	**49**	**67.6**

Table 4.5 Temperature obtained through experiment at speed: 150 rpm, doc: 0.1 mm

Sl No	Time [s]	Max Temp [°C]
1	0.49	30.196
2	0.75705	30.303
3	0.92899	30.372
4	1.1009	30.44
5	1.6167	30.647
6	2.7593	31.104
7	5.6417	32.257
8	10.542	34.217
9	15.442	36.204
10	20.342	38.465
11	25.242	40.727
12	30.142	45.427
13	35.042	52.45
14	39.942	58.913
15	44.842	61.905
16	**49**	**69**

Table 4.6 Temperature obtained through FEA at speed: 150 rpm, doc: 0.1 mm

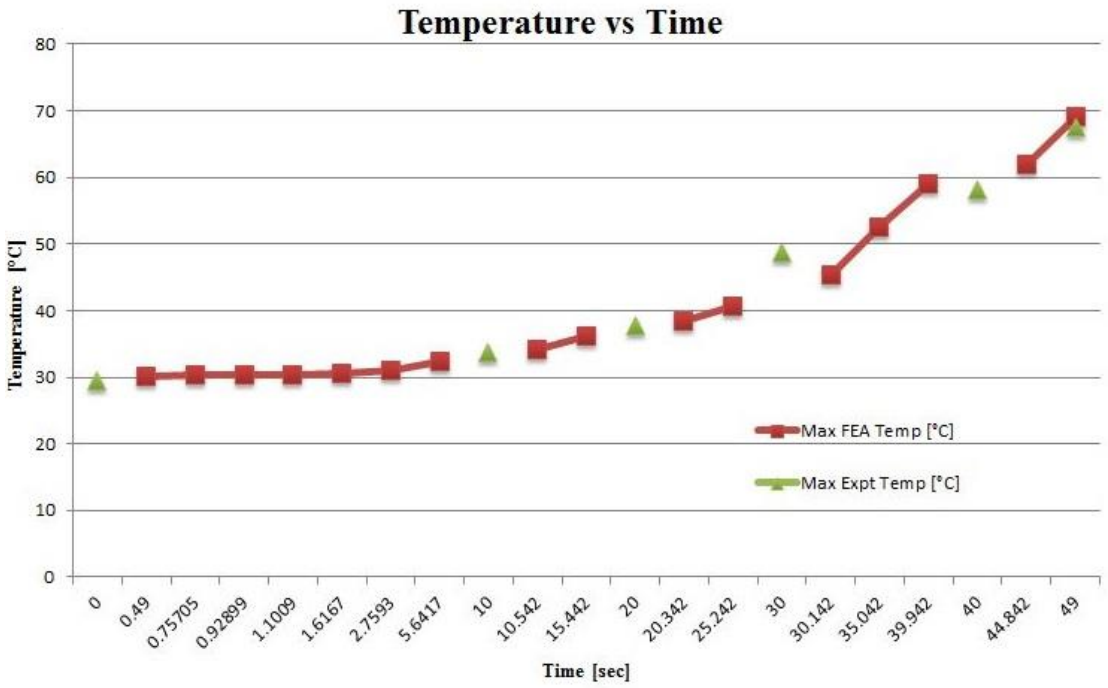

Figure 4.1 Comparison of temperatures at speed: 150 rpm, doc: 0.1 mm

From the graph it is clear that temperature increases when machining progresses. The temperatures obtained through FEA and experiment having almost same values. The percentage difference between maximum temperatures obtained at machining end time is only 2.03%.

4.5.2 TEMPERATURE OBTAINED AT SPEED: 150 rpm, DOC: 0.4 mm

Sl No	Time [sec]	Max Temp [°C]
1	0	57
2	10	70.8
3	20	81.8
4	30	91
5	40	99.6
6	**49**	**104.4**

Table 4.7 Temperature obtained through experiment at speed: 150 rpm, doc: 0.4 mm

Sl No	Time [s]	Max Temp [°C]
1	0.49	59.294
2	0.75831	59.455
3	0.91568	59.549
4	1.073	59.644
5	1.5176	59.911
6	2.3235	60.394
7	3.8775	61.327
8	7.1347	63.281
9	12.035	67.849
10	16.935	74.084
11	21.835	79.361
12	26.735	84.637
13	31.635	88.908
14	36.535	92.121
15	41.435	97.148
16	46.335	102.67
17	**49**	**108**

Table 4.8 Temperature obtained through FEA at speed: 150 rpm, doc: 0.4 mm

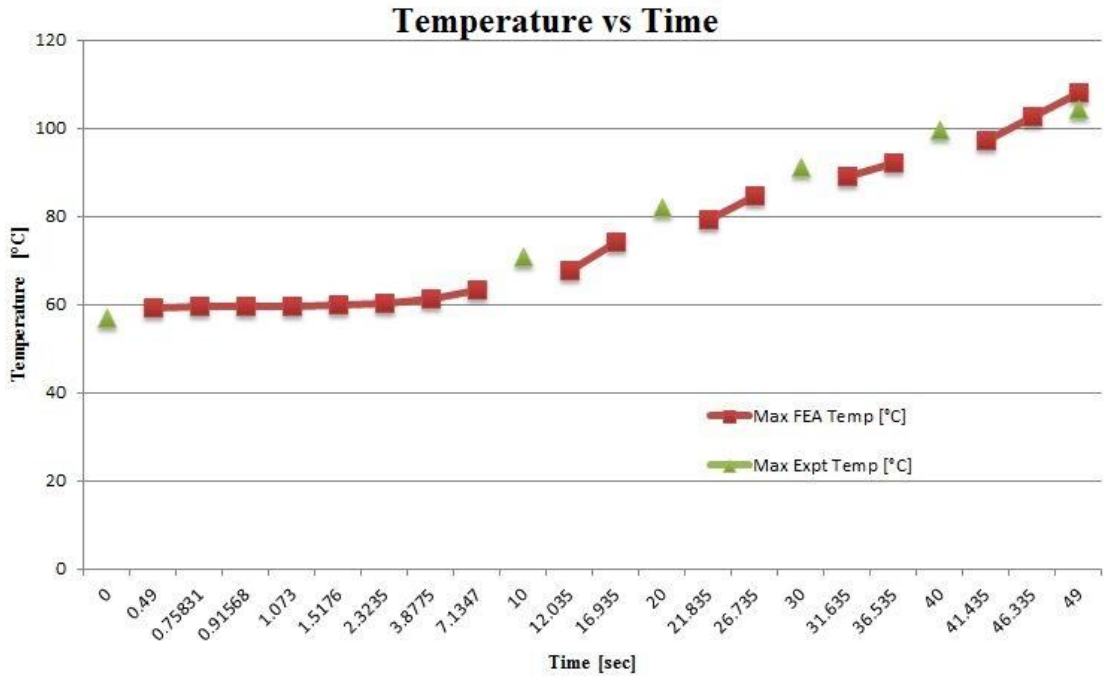

Figure 4.2 Comparison of temperatures at speed: 150 rpm, doc: 0.4 mm

From the graph it is clear that temperature increases when machining progresses. The temperatures obtained through FEA and experiment having almost same values. The percentage difference between maximum temperatures obtained at machining end time is only 3.33%.

4.5.3 TEMPERATURE OBTAINED AT SPEED: 150 rpm, DOC: 0.7 mm

Sl No	Time [sec]	Max Temp [°C]
1	0	100.9
2	10	115.2
3	20	126.8
4	30	135.4
5	40	147.2
6	**49**	**152.4**

Table 4.9 Temperature obtained through experiment at speed: 150 rpm, doc: 0.7 mm

Sl No	Time [s]	Max Temp [°C]
1	0.49	100.49
2	0.75828	100.76
3	0.91381	100.91
4	1.0693	101.07
5	1.5031	101.5
6	2.2779	102.28
7	3.7343	103.73
8	6.6561	106.66
9	11.556	113.11
10	16.456	121.79
11	21.356	127.82
12	26.256	133.85
13	31.156	139.79
14	36.056	145.67
15	40.956	149.19
16	45.856	151.07
17	**49**	**155**

Table 4.10 Temperature obtained through FEA at speed: 150 rpm, doc: 0.7 mm

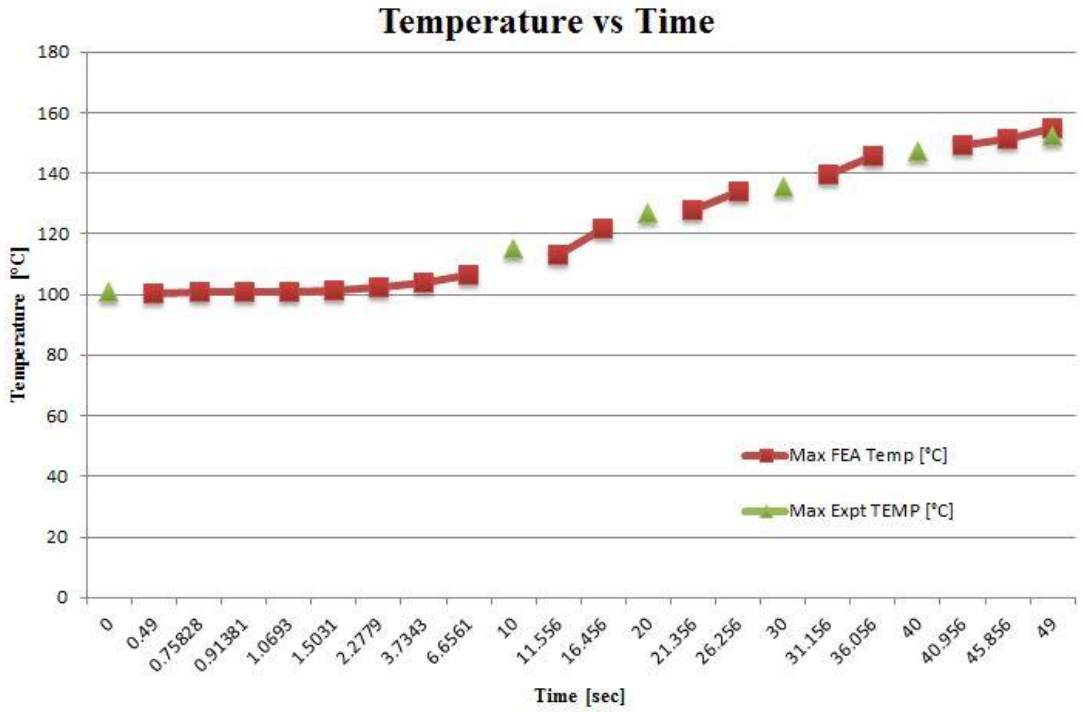

Figure 4.3 Comparison of temperatures at speed: 150 rpm, doc: 0.7 mm

From the graph it is clear that temperature increases when machining progresses. The temperatures obtained through FEA and experiment having almost same values. The percentage difference between maximum temperatures obtained at machining end time is only 1.68%.

4.5.4 TEMPERATURE OBTAINED AT SPEED: 420 rpm, DOC: 0.1 mm

Sl No	Time [sec]	Max Temp [°C]
1	0	41.4
2	5	56
3	10	72.2
4	**17.5**	**78.4**

Table 4.11 Temperature obtained through experiment at speed: 420 rpm, doc: 0.1 mm

Sl No	Time [s]	Max Temp [°C]
1	0.175	42.292
2	0.27753	42.463
3	0.34551	42.576
4	0.41349	42.689
5	0.59411	42.99
6	0.9036	43.506
7	1.4888	44.481
8	2.8064	46.677
9	4.5564	54.004
10	6.3064	57.96
11	8.0564	60.056
12	9.8064	61.806
13	11.556	63.649
14	13.306	65.691
15	15.056	67.732
16	16.806	69.774
17	**17.5**	**77**

Table 4.12 Temperature obtained through FEA at speed: 420 rpm, doc: 0.1 mm

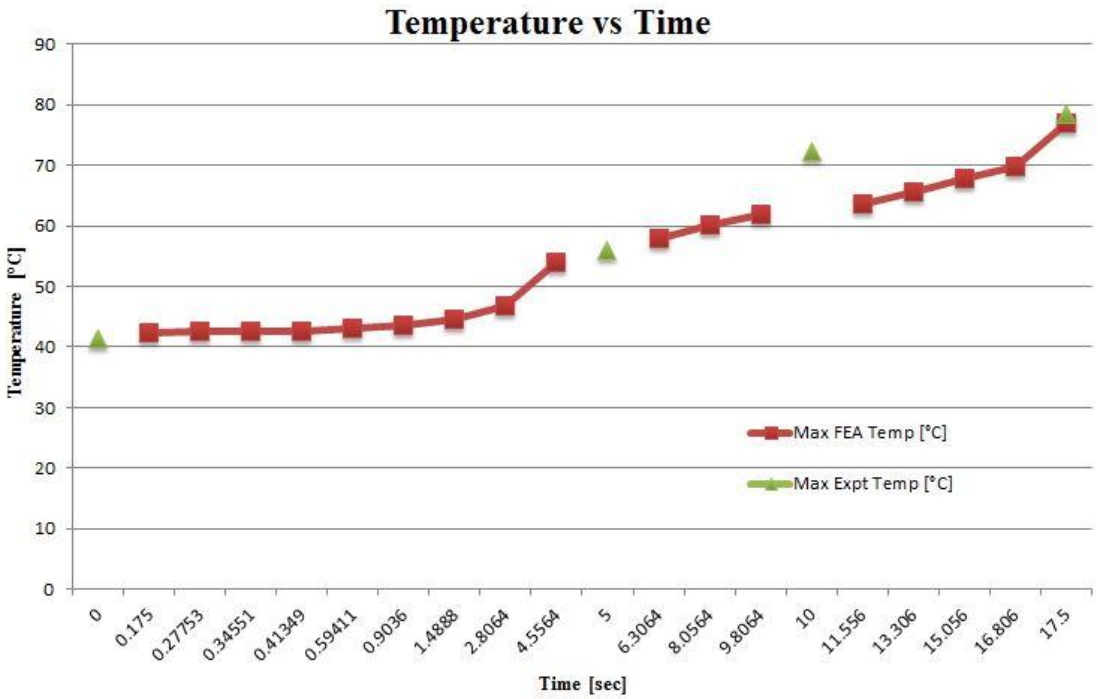

Figure 4.4 Comparison of temperatures at speed: 420 rpm, doc: 0.1 mm

From the graph it is clear that temperature increases when machining progresses. The temperatures obtained through FEA and experiment having almost same values. The percentage difference between maximum temperatures obtained at machining end time is only 1.79%.

4.5.5 TEMPERATURE OBTAINED AT SPEED: 420 rpm, DOC: 0.4 mm

Sl No	Time [sec]	Max Temp [°C]
1	0	72.6
2	5	81.8
3	10	94.8
4	**17.5**	**109.6**

Table 4.13 Temperature obtained through experiment at speed: 420 rpm, doc: 0.4 mm

Sl No	Time [s]	Max Temp [°C]
1	0.175	74.35
2	0.27721	74.554
3	0.34151	74.683
4	0.40581	74.812
5	0.56679	75.134
6	0.8242	75.648
7	1.2557	76.511
8	2.0436	78.087
9	3.69	82.07
10	5.44	87.32
11	7.19	92.285
12	8.94	94.91
13	10.69	97.535
14	12.44	100.88
15	14.19	104.38
16	15.94	107.88
17	**17.5**	**112**

Table 4.14 Temperature obtained through FEA at speed: 420 rpm, doc: 0.4 mm

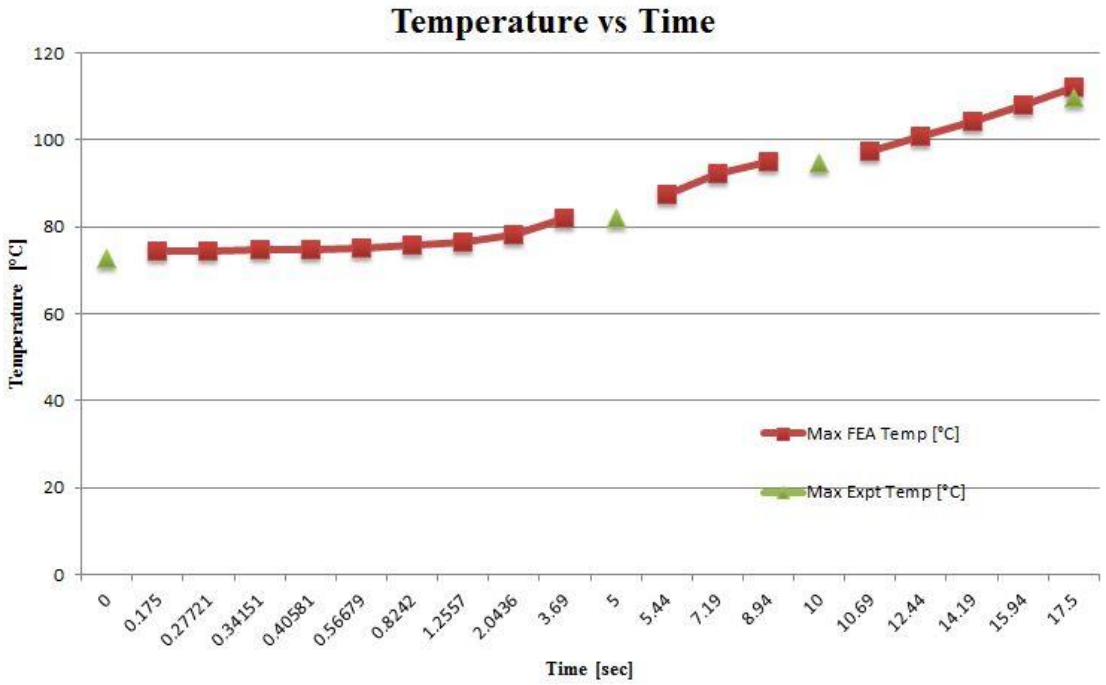

Figure 4.5 Comparison of temperatures at speed: 420 rpm, doc: 0.4 mm

From the graph it is clear that temperature increases when machining progresses. The temperatures obtained through FEA and experiment having almost same values. The percentage difference between maximum temperatures obtained at machining end time is only 2.14%.

4.5.6 TEMPERATURE OBTAINED AT SPEED: 420 rpm, DOC: 0.7 mm

Sl No	Time [sec]	Max Temp [°C]
1	0	111
2	5	130.2
3	10	146
4	**17.5**	**158.6**

Table 4.15 Temperature obtained through experiment at speed: 420 rpm, doc: 0.7 mm

Sl No	Time [s]	Max Temp [°C]
1	0.175	112.47
2	0.27793	112.74
3	0.34225	112.91
4	0.40658	113.08
5	0.56548	113.51
6	0.81625	114.18
7	1.2278	115.27
8	1.9534	117.21
9	3.3809	121.52
10	5.1309	128.46
11	6.8809	134.58
12	8.6309	139.49
13	10.381	144.3
14	12.131	148.26
15	13.881	151.76
16	15.631	155.26
17	16.565	157.13
18	**17.5**	**160**

Table 4.16 Temperature obtained through FEA at speed: 420 rpm, doc: 0.7 mm

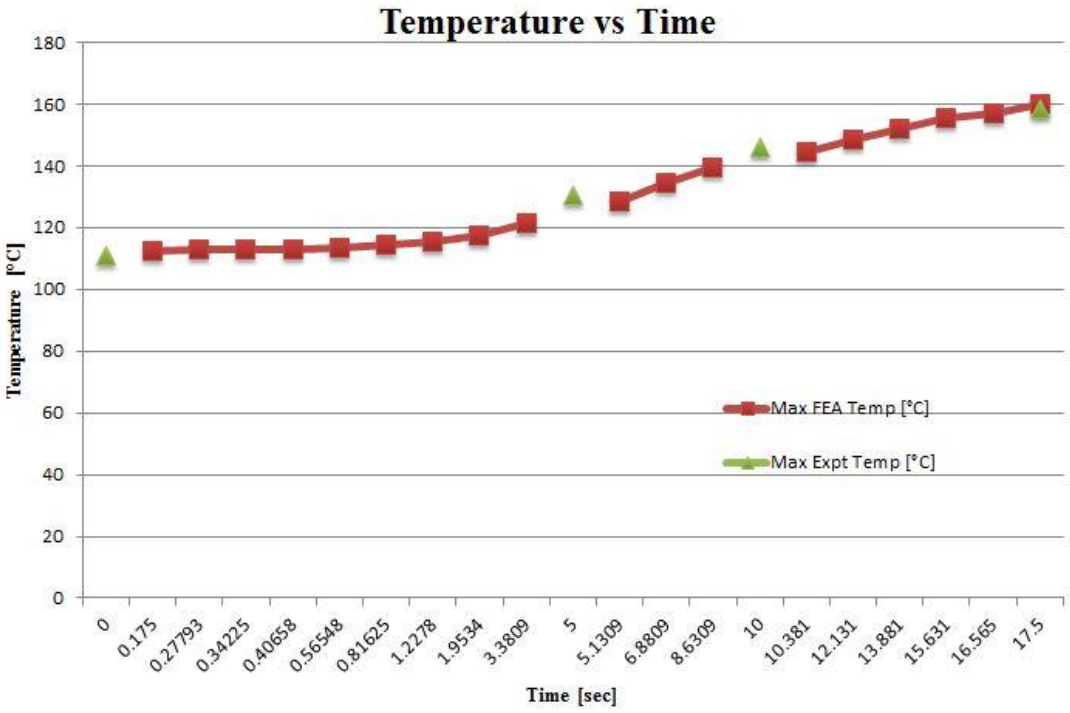

Figure 4.6 Comparison of temperatures at speed: 420 rpm, doc: 0.7 mm

From the graph it is clear that temperature increases when machining progresses. The temperatures obtained through FEA and experiment having almost same values. The percentage difference between maximum temperatures obtained at machining end time is only 0.875%.

4.5.7 TEMPERATURE OBTAINED AT SPEED: 710 rpm, DOC: 0.1 mm

Sl No	Time [sec]	Max Temp [°C]
1	0	50.2
2	5	63.8
3	**10**	**81.6**

Table 4.17 Temperature obtained through experiment at speed: 710 rpm, doc: 0.1 mm

Sl No	Time [s]	Max Temp [°C]
1	0.1	51.35
2	0.15862	51.555
3	0.19996	51.7
4	0.24129	51.845
5	0.34897	52.221
6	0.52556	52.839
7	0.83124	53.909
8	1.4347	56.021
9	2.4347	60.608
10	3.4347	64.652
11	4.4347	66.152
12	5.4347	67.652
13	6.4347	69.152
14	7.4347	72.608
15	8.4346	77.739
16	9.4346	81.739
17	**10**	**84**

Table 4.18 Temperature obtained through FEA at speed: 710 rpm, doc: 0.1 mm

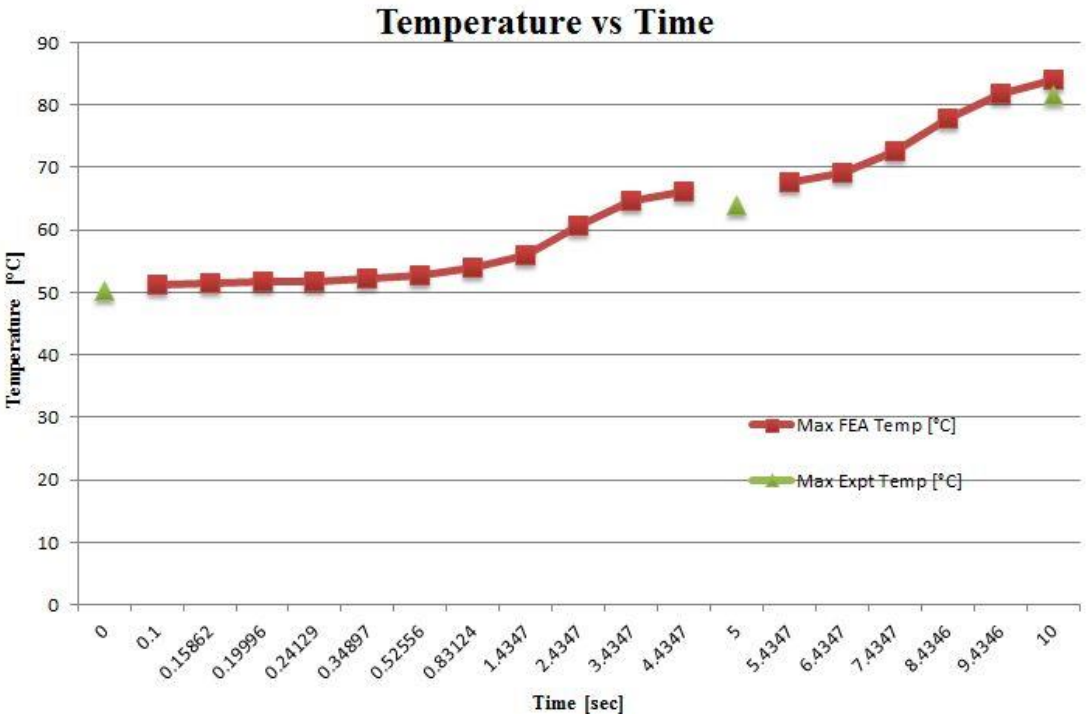

Figure 4.7 Comparison of temperatures at speed: 710 rpm, doc: 0.1 mm

From the graph it is clear that temperature increases when machining progresses. The temperatures obtained through FEA and experiment having almost same values. The percentage difference between maximum temperatures obtained at machining end time is only 2.85%.

4.5.8 TEMPERATURE OBTAINED AT SPEED: 710 rpm, DOC: 0.4 mm

Sl No	Time [sec]	Max Temp [°C]
1	0	80.6
2	5	103.4
3	**10**	**124.6**

Table 4.19 Temperature obtained through experiment at speed: 710 rpm, doc: 0.4 mm

Sl No	Time [s]	Max Temp [°C]
1	0.1	80.25
2	0.15935	80.398
3	0.19934	80.498
4	0.23933	80.598
5	0.33729	80.843
6	0.4871	81.218
7	0.71899	81.797
8	1.0974	82.743
9	1.7719	84.43
10	2.7719	91.175
11	3.7719	96.087
12	4.7719	100.09
13	5.7719	104.09
14	6.7719	108.09
15	7.7719	113.63
16	8.7719	119.63
17	9.3859	123.32
18	**10**	**127**

Table 4.20 Temperature obtained through FEA at speed: 710 rpm, doc: 0.4 mm

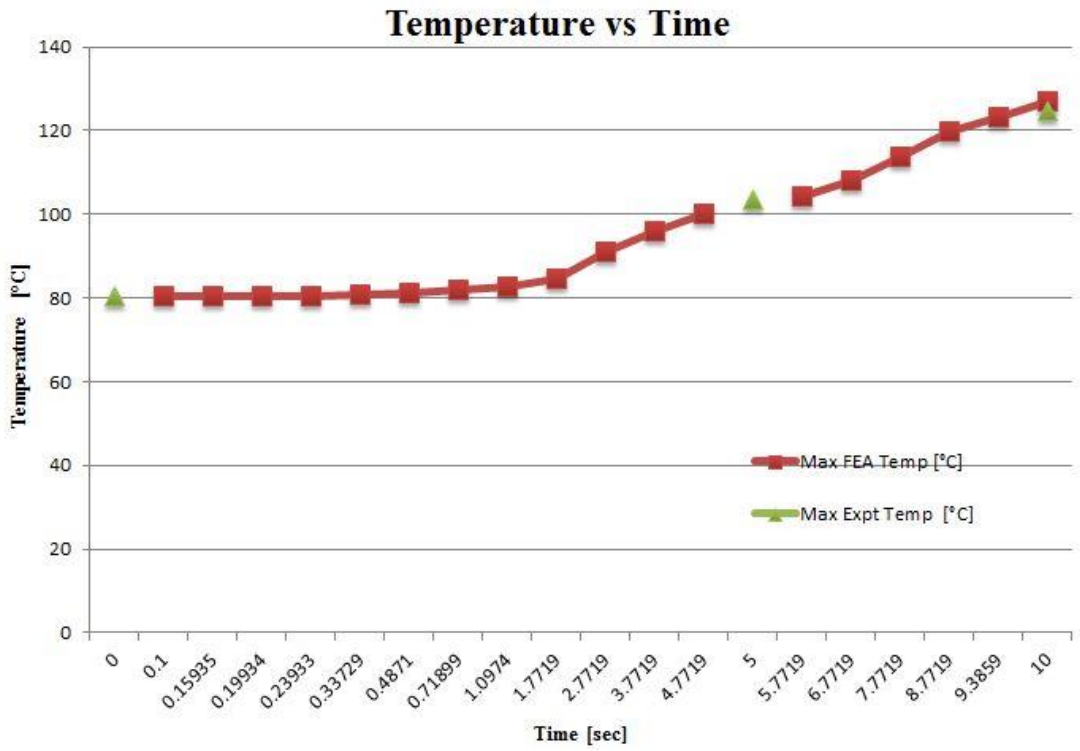

Figure 4.8 Comparison of temperatures at speed: 710 rpm, doc: 0.4 mm

From the graph it is clear that temperature increases when machining progresses. The temperatures obtained through FEA and experiment having almost

same values. The percentage difference between maximum temperatures obtained at machining end time is only 1.89%.

4.5.9 TEMPERATURE OBTAINED AT SPEED: 710 rpm, DOC: 0.7 mm

Sl No	Time [sec]	Max Temp [°C]
1	0	123.4
2	5	139.2
3	**10**	**167.6**

Table 4.21 Temperature obtained through experiment at speed: 710 rpm, doc: 0.7 mm

Sl No	Time [s]	Max Temp [°C]
1	0.1	122.7
2	0.1591	123.11
3	0.19918	123.39
4	0.23925	123.67
5	0.34013	124.38
6	0.49807	125.49
7	0.75149	127.26
8	1.1908	130.34
9	2.0586	136.41
10	3.0586	143.18
11	4.0586	146.18
12	5.0586	149.18
13	6.0586	152.18
14	7.0586	155.59
15	8.0586	165.15
16	9.0586	167.65
17	**10**	**170**

Table 4.22 Temperature obtained through FEA at speed: 710 rpm, doc: 0.7 mm

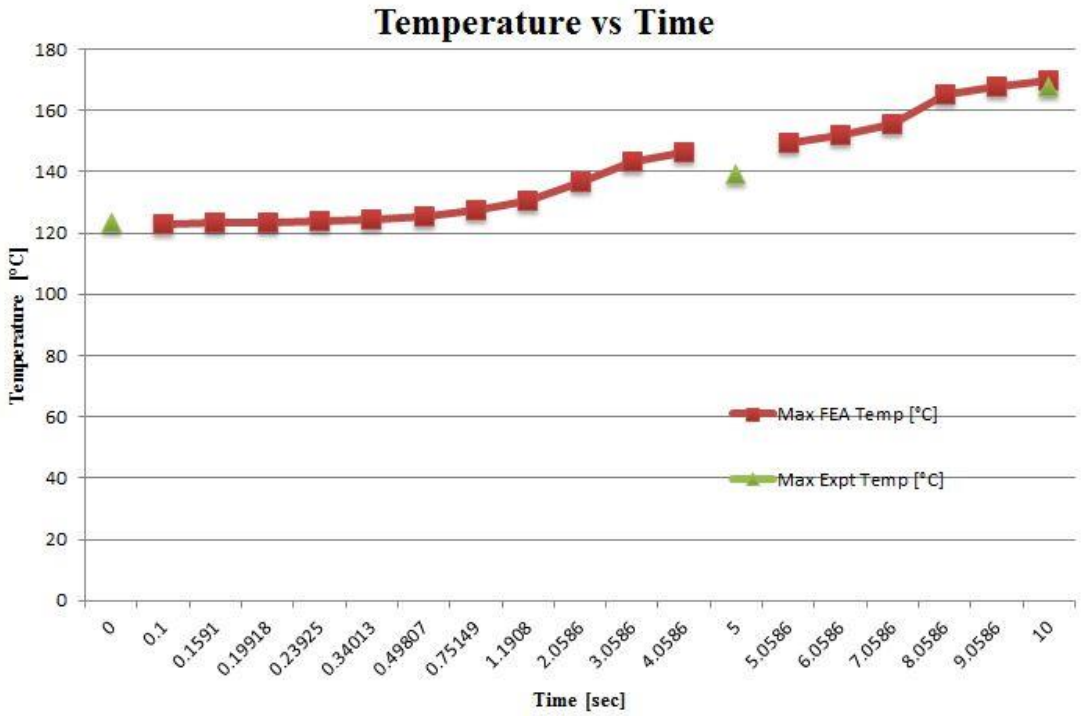

Figure 4.9 Comparison of temperatures at speed: 710 rpm, doc: 0.7 mm

From the graph it is clear that temperature increases when machining progresses. The temperatures obtained through FEA and experiment having almost same values. The percentage difference between maximum temperatures obtained at machining end time is only 1.41%.

4.6 EXPERIMENTAL AND FINITE ELEMENT ANALYSIS RESULTS FOR CARBIDE TOOL

The temperatures obtained for carbide tool at various speed and depth of cut through experiment and FEA are summarized in Tables and graphs given below.

4.6.1 TEMPERATURE OBTAINED AT SPEED: 150 rpm, DOC: 0.1 mm

Sl No	Time [sec]	Max Temp [°C]
1	0	32
2	10	38.6
3	20	45.6
4	30	55
5	40	62.8
6	**49**	**75.4**

Table 4.23 Temperature obtained through experiment at speed: 150 rpm, doc: 0.1 mm

Sl No	Time [s]	Max Temp [°C]
1	0.49	32.343
2	0.65333	32.463
3	0.81667	32.577
4	1.1864	32.836
5	1.943	33.365
6	3.4939	34.451
7	6.0632	36.25
8	9.0972	38.375
9	12.442	41.45
10	14.803	43.812
11	17.132	46.723
12	18.943	49.028
13	20.753	51.334
14	23.066	54.278
15	25.747	57.691
16	28.867	59.578
17	33.767	62.252
18	38.667	65.822
19	43.567	71.132
20	46.284	74.076
21	**49**	**77.02**

Table 4.24 Temperature obtained through FEA at speed: 150 rpm, doc: 0.1 mm

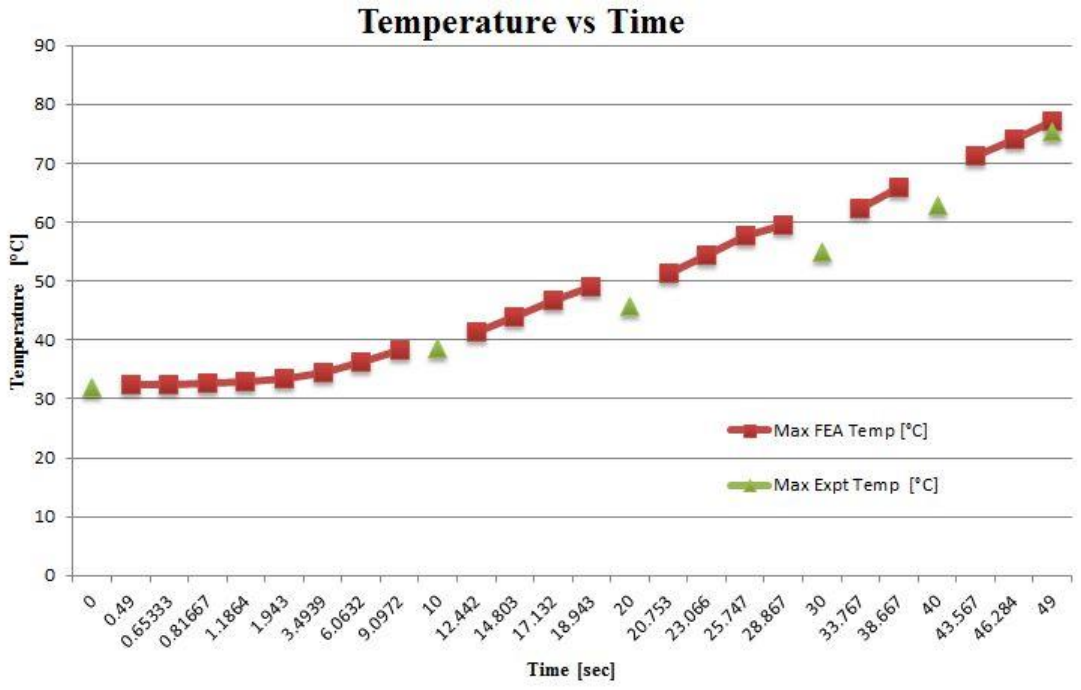

Figure 4.10 Comparison of temperatures at speed: 150 rpm, doc: 0.1 mm

From the graph it is clear that temperature increases when machining progresses. The temperatures obtained through FEA and experiment having almost same values. The percentage difference between maximum temperatures obtained at machining end time is only 2.10%.

4.6.2 TEMPERATURE OBTAINED AT SPEED: 150 rpm, DOC: 0.4 mm

Sl No	Time [sec]	Max Temp [°C]
1	0	61
2	10	71.8
3	20	83.2
4	30	93
5	40	100.8
6	**49**	**111.8**

Table 4.25 Temperature obtained through experiment at speed: 150 rpm, doc: 0.4 mm

Sl No	Time [s]	Max Temp [°C]
1	0.49	60.637
2	0.65333	60.87
3	0.81057	61.074
4	0.96781	61.278
5	1.4395	61.89
6	2.422	63.167
7	4.7288	66.167
8	9.6288	72.538
9	14.529	83.893
10	17.878	86.596
11	21.228	88.423
12	26.128	91.177
13	31.028	96.969
14	35.928	102.76
15	40.828	107.54
16	45.728	112.03
17	**49**	**115.03**

Table 4.26 Temperature obtained through FEA at speed: 150 rpm, doc: 0.4 mm

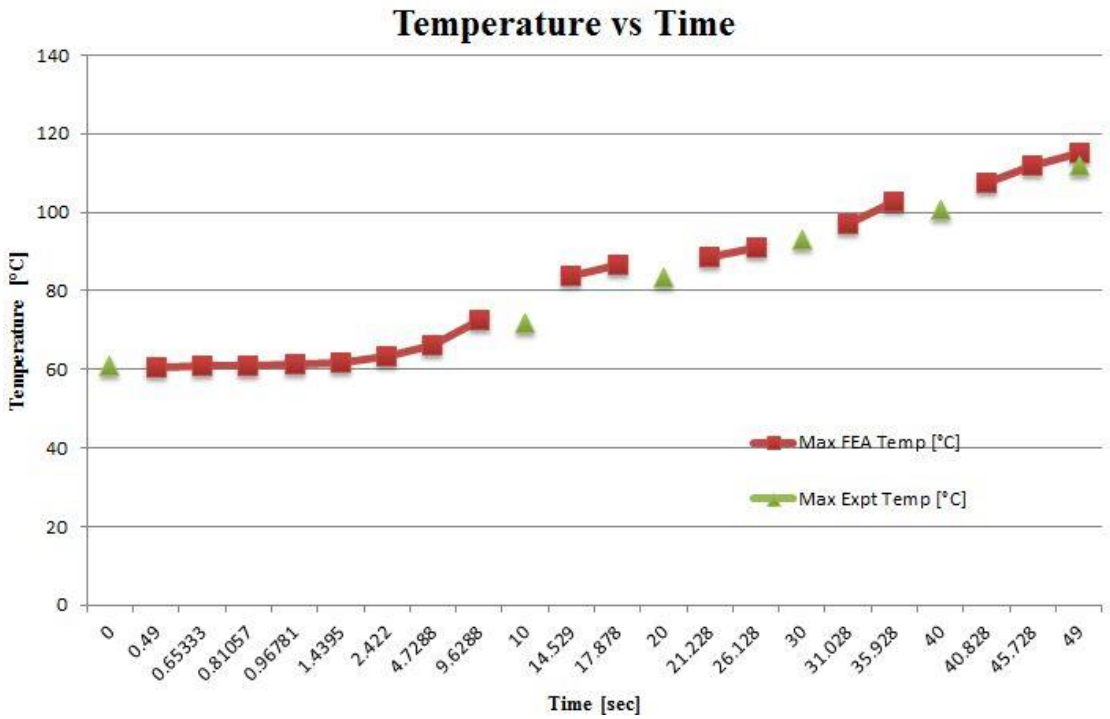

Figure 4.11 Comparison of temperatures at speed: 150 rpm, doc: 0.4 mm

From the graph it is clear that temperature increases when machining progresses. The temperatures obtained through FEA and experiment having almost same values. The percentage difference between maximum temperatures obtained at machining end time is only 2.81%.

4.6.3 TEMPERATURE OBTAINED AT SPEED: 150 rpm, DOC: 0.7 mm

Sl No	Time [sec]	Max Temp [°C]
1	0	101.2
2	10	119
3	20	130.2
4	30	138.8
5	40	151.2
6	**49**	**159.4**

Table 4.27 Temperature obtained through experiment at speed: 150 rpm, doc: 0.7 mm

Sl No	Time [s]	Max Temp [°C]
1	0.49	102.88
2	0.65333	103.22
3	0.80639	103.49
4	0.95945	103.77
5	1.4186	104.59
6	2.3269	106.23
7	4.4218	110
8	9.3218	118.82
9	14.222	126.8
10	19.122	132.91
11	24.022	138.71
12	28.922	144.23
13	33.822	149.58
14	38.722	154.34
15	43.622	158.01
16	46.311	160.03
17	**49**	**162.05**

Table 4.28 Temperature obtained through FEA at speed: 150 rpm, doc: 0.7 mm

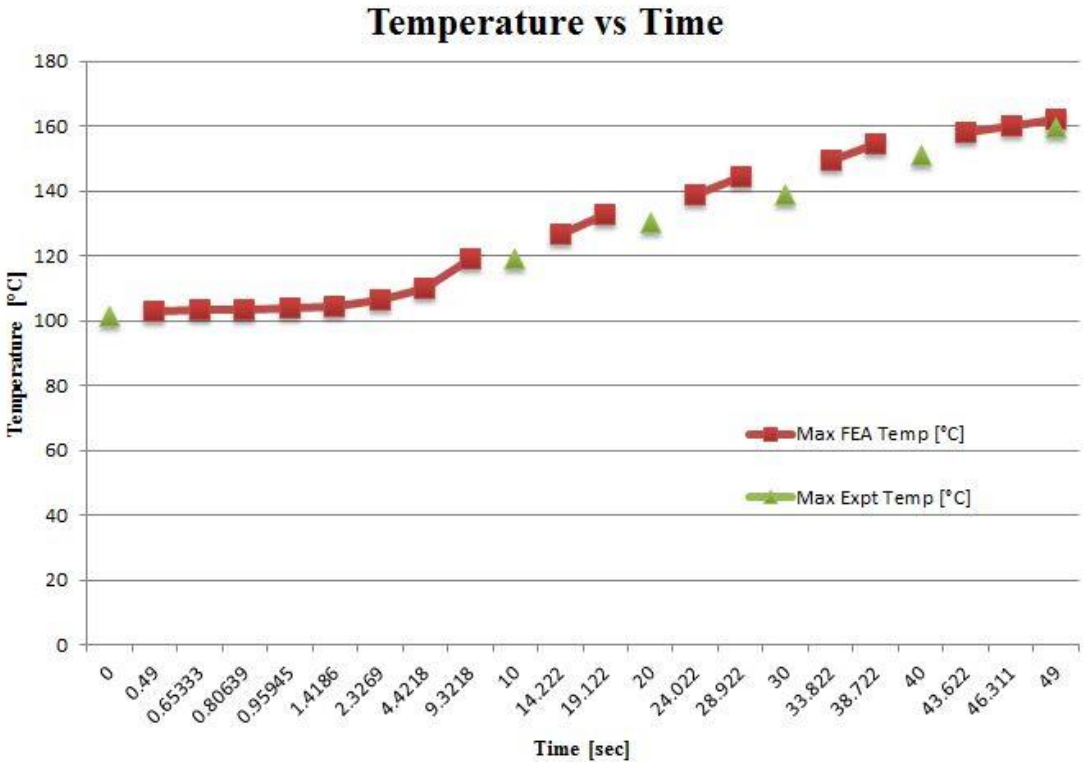

Figure 4.12 Comparison of temperatures at speed: 150 rpm, doc: 0.7 mm

From the graph it is clear that temperature increases when machining progresses. The temperatures obtained through FEA and experiment having almost

same values. The percentage difference between maximum temperatures obtained at machining end time is only 1.64%

. **4.6.4 TEMPERATURE OBTAINED AT SPEED: 420 rpm, DOC: 0.1 mm**

Sl No	Time [sec]	Max Temp [°C]
1	0	43.8
2	5	60.2
3	10	75.8
4	**17.5**	**82.8**

Table 4.29 Temperature obtained through experiment at speed: 420 rpm, doc: 0.1 mm

Sl No	Time [s]	Max Temp [°C]
1	0.175	42.315
2	0.23333	42.432
3	0.28728	42.529
4	0.34123	42.625
5	0.50307	42.916
6	0.79478	43.441
7	1.329	44.402
8	2.3382	46.219
9	4.0233	49.253
10	5.7733	52.404
11	7.5233	55.556
12	9.2733	58.707
13	11.023	63.7
14	12.259	68.15
15	13.209	71.571
16	14.159	74.992
17	15.375	79.071
18	16.94	83.456
19	**17.5**	**85.025**

Table 4.30 Temperature obtained through FEA at speed: 420 rpm, doc: 0.1 mm

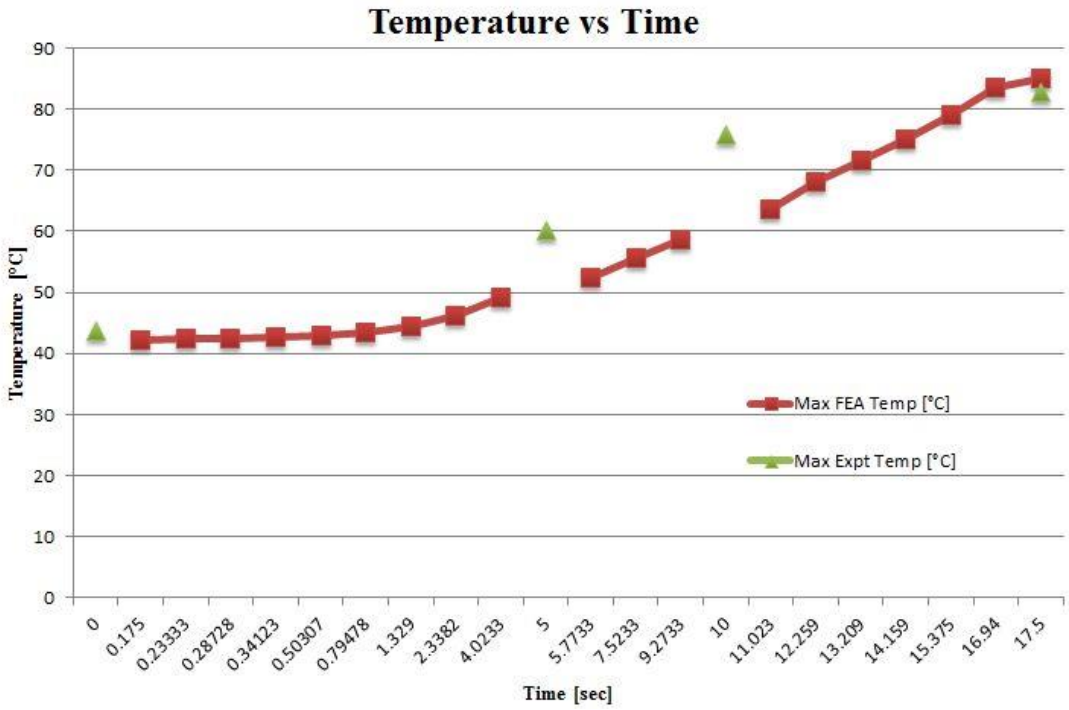

Figure 4.13 Comparison of temperatures at speed: 420 rpm, doc: 0.1 mm

From the graph it is clear that temperature increases when machining progresses. The temperatures obtained through FEA and experiment having almost same values. The percentage difference between maximum temperatures obtained at machining end time is only 2.62%.

4.6.5 TEMPERATURE OBTAINED AT SPEED: 420 rpm, DOC: 0.4 mm

Sl No	Time [sec]	Max Temp [°C]
1	0	71.4
2	5	85.8
3	10	103
4	**17.5**	**119.2**

Table 4.31 Temperature obtained through experiment at speed: 420 rpm, doc: 0.4 mm

Sl No	Time [s]	Max Temp [°C]
1	0.175	72.28
2	0.23333	72.404
3	0.2847	72.486
4	0.33607	72.567
5	0.48541	72.804
6	0.73342	73.2
7	1.1535	73.871
8	1.9184	75.094
9	3.5475	77.701
10	5.2975	80.501
11	7.0475	83.302
12	8.7975	86.102
13	10.548	89.779
14	12.298	95.381
15	14.048	100.98
16	15.798	108.18
17	**17.5**	**117.04**

Table 4.32 Temperature obtained through FEA at speed: 420 rpm, doc: 0.4 mm

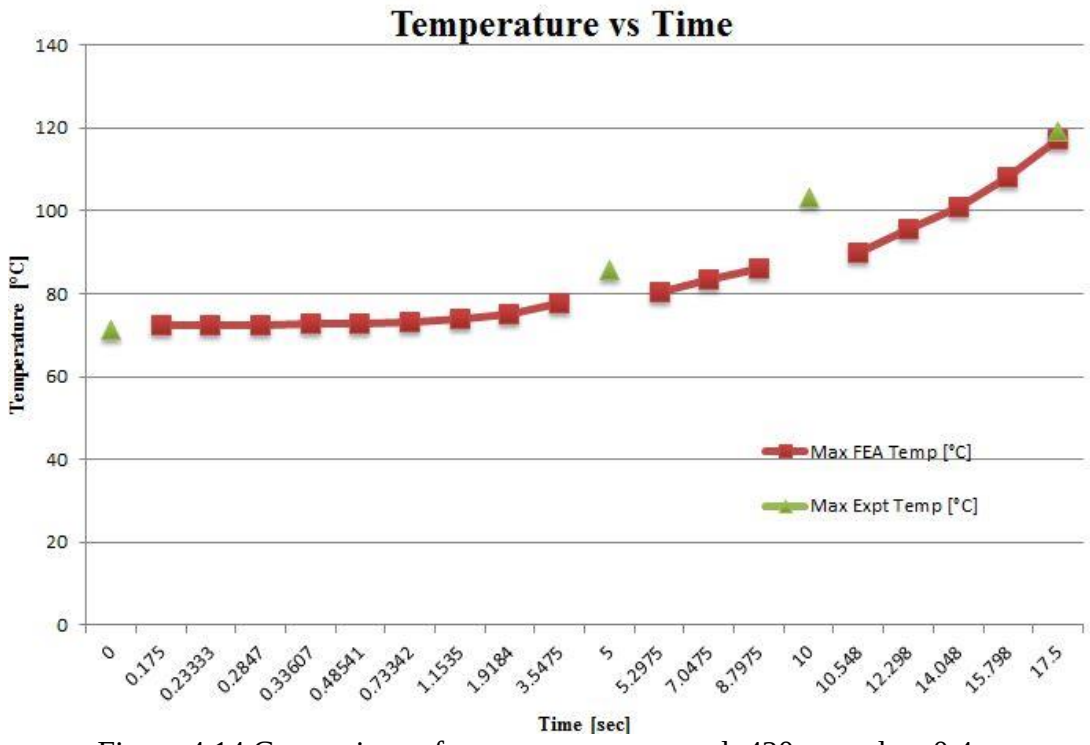

Figure 4.14 Comparison of temperatures at speed: 420 rpm, doc: 0.4 mm

From the graph it is clear that temperature increases when machining progresses. The temperatures obtained through FEA and experiment having almost same values. The percentage difference between maximum temperatures obtained at machining end time is only 6.36%.

4.6.6 TEMPERATURE OBTAINED AT SPEED: 420 rpm, DOC: 0.7 mm

Sl No	Time [sec]	Max Temp [°C]
1	0	111.2
2	5	136
3	10	153.6
4	**17.5**	**167.6**

Table 4.33 Temperature obtained through experiment at speed: 420 rpm, doc: 0.7 mm

Sl No	Time [s]	Max Temp [°C]
1	0.175	111.46
2	0.23333	111.66
3	0.28458	111.8
4	0.33582	111.93
5	0.48437	112.31
6	0.73025	112.95
7	1.1447	114.02
8	1.8936	115.97
9	3.4758	120.08
10	5.2258	124.63
11	6.9758	129.18
12	8.7258	133.73
13	10.476	138.86
14	12.226	145.51
15	13.976	152.16
16	15.726	159.83
17	**17.5**	**169.06**

Table 4.34 Temperature obtained through FEA at speed: 420 rpm, doc: 0.7 mm

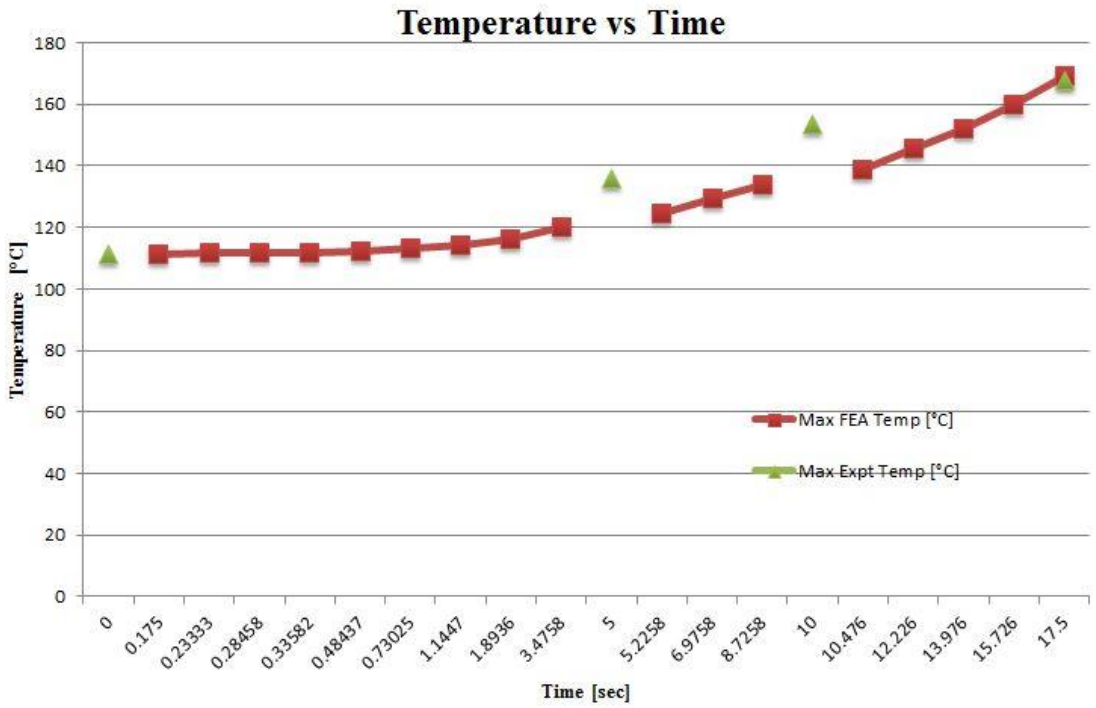

Figure 4.15 Comparison of temperatures at speed: 420 rpm, doc: 0.7 mm

From the graph it is clear that temperature increases when machining progresses. The temperatures obtained through FEA and experiment having almost same values. The percentage difference between maximum temperatures obtained at machining end time is only 0.86%.

4.6.7 TEMPERATURE OBTAINED AT SPEED: 710 rpm, DOC: 0.1 mm

Sl No	Time [sec]	Max Temp [°C]
1	0	54.2
2	5	67.8
3	**10**	**86.8**

Table 4.35 Temperature obtained through experiment at speed: 710 rpm, doc: 0.1 mm

Sl No	Time [s]	Max Temp [°C]
1	0.1	51.38
2	0.13333	51.523
3	0.16263	51.636
4	0.19192	51.747
5	0.27981	52.079
6	0.43652	52.674
7	0.71219	53.721
8	1.2147	55.63
9	2.0944	58.974
10	3.0944	62.775
11	4.0944	66.577
12	5.0944	70.397
13	6.0944	74.399
14	7.0944	78.4
15	8.0944	82.402
16	9.0944	86.403
17	**10**	**90.027**

Table 4.36 Temperature obtained through FEA at speed: 710 rpm, doc: 0.1 mm

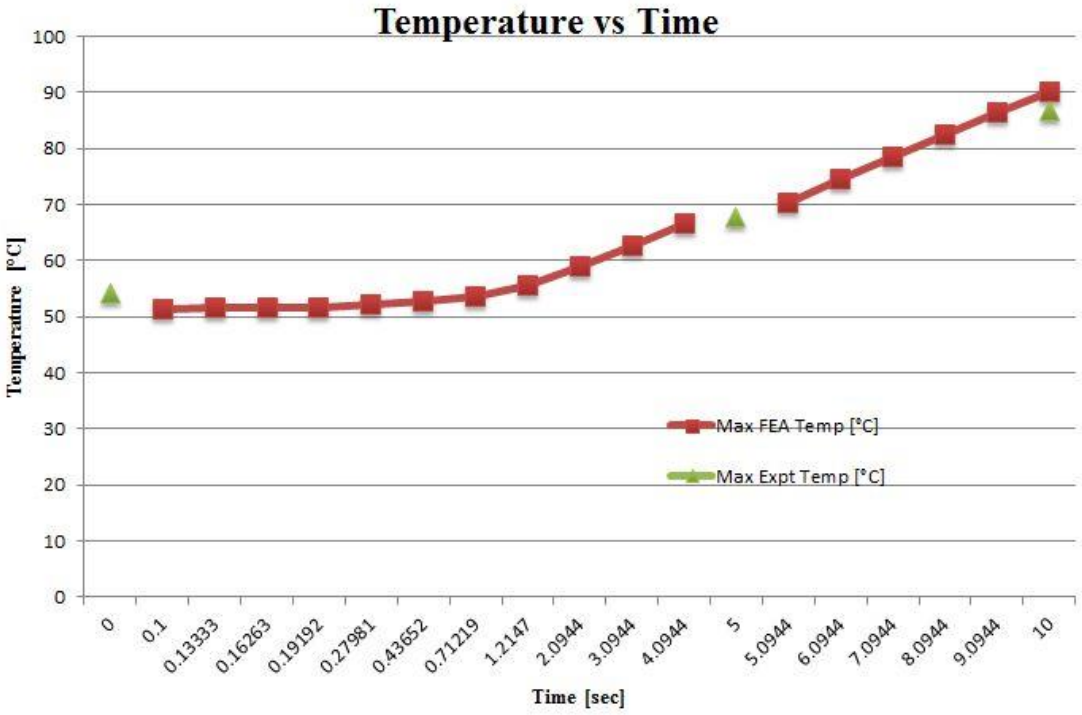

Figure 4.16 Comparison of temperatures at speed: 710 rpm, doc: 0.1 mm

From the graph it is clear that temperature increases when machining progresses. The temperatures obtained through FEA and experiment having almost

same values. The percentage difference between maximum temperatures obtained at machining end time is only 3.58%.

4.6.8 TEMPERATURE OBTAINED AT SPEED: 710 rpm, DOC: 0.4 mm

Sl No	Time [sec]	Max Temp [°C]
1	0	81
2	5	107.8
3	10	127

Table 4.37 Temperature obtained through experiment at speed: 710 rpm, doc: 0.4mm

Sl No	Time [s]	Max Temp [°C]
1	0.1	83.54
2	0.13333	83.756
3	0.16203	83.915
4	0.19073	84.068
5	0.27682	84.53
6	0.42369	85.321
7	0.6731	86.666
8	1.1153	89.053
9	1.9424	93.52
10	2.9424	98.921
11	3.9424	104.32
12	4.9424	109.73
13	5.9424	113.62
14	6.9424	117.42
15	7.9424	121.22
16	8.9424	125.02
17	9.4712	127.03
18	**10**	**129.04**

Table 4.38 Temperature obtained through FEA at speed: 710 rpm, doc: 0.4 mm

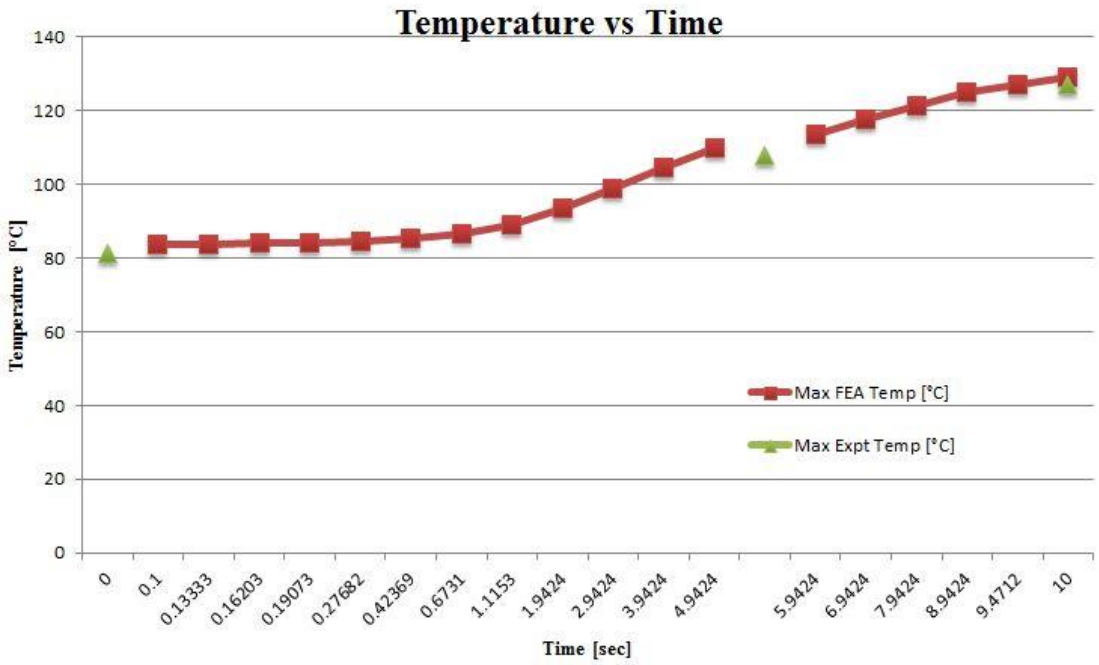

Figure 4.17 Comparison of temperatures at speed: 710 rpm, doc: 0.4 mm

From the graph it is clear that temperature increases when machining progresses. The temperatures obtained through FEA and experiment having almost same values. The percentage difference between maximum temperatures obtained at machining end time is only 1.58%.

4.6.9 TEMPERATURE OBTAINED AT SPEED: 710 rpm, DOC: 0.7 mm

Sl No	Time [sec]	Max Temp [°C]
1	0	126
2	5	144.4
3	10	175.2

Table 4.39 Temperature obtained through experiment at speed: 710 rpm, doc: 0.7 mm

Sl No	Time [s]	Max Temp [°C]
1	0.1	125.46
2	0.13333	125.68
3	0.16142	125.81
4	0.18951	125.94
5	0.27271	126.32
6	0.40929	126.94
7	0.6316	127.96
8	1.0041	129.67
9	1.673	132.75
10	2.673	137.35
11	3.673	141.95
12	4.673	146.55
13	5.673	151.55
14	6.673	156.76
15	7.673	161.96
16	8.673	167.16
17	9.3365	170.61
18	**10**	**174.06**

Table 4.40 Temperature obtained through FEA at speed: 710 rpm, doc: 0.7 mm

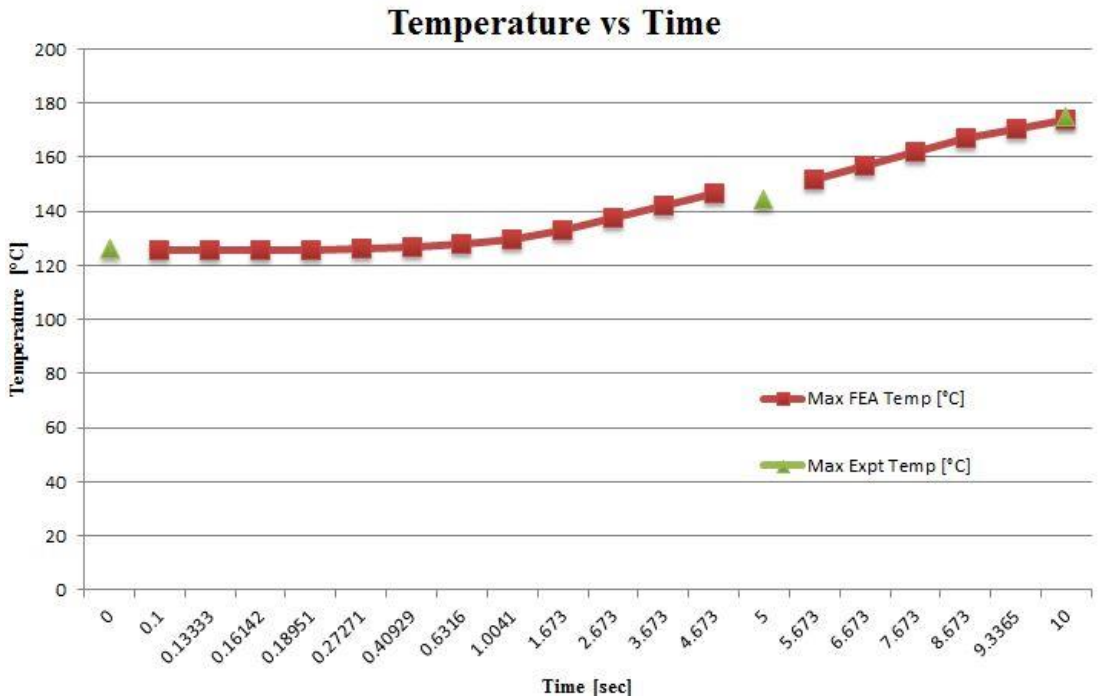

Figure 4.18 Comparison of temperatures at speed: 710 rpm, doc: 0.7 mm

From the graph it is clear that temperature increases when machining progresses. The temperatures obtained through FEA and experiment having almost same values. The percentage difference between maximum temperatures obtained at machining end time is only 0.65%.

4.7 PERCENTAGE DIFFERENCE BETWEEN MAXIMUM TEMPERATURES OBTAINED THROUGH EXPERIMENT AND FEA FOR HSS TOOL

Sl No	Feed (mm per rev)	Speed (rpm)	Machining Time (sec)	Depth of Cut (mm)	Max Expt Temp (°C)	Max FEA Temp (°C)	Percentage Difference (%)
1	0.52	150	49	0.1	67.6	69	2.03
2				0.4	104.4	108	3.33
3				0.7	152.4	155	1.68
4		420	17.5	0.1	78.4	77	1.79
5				0.4	109.6	112	2.14
6				0.7	158.6	160	0.875
7		710	10	0.1	81.6	84	2.85
8				0.4	124.6	127	1.89
9				0.7	167.6	170	1.41

Table 4.41 Percentage difference between max temperatures obtained for HSS tool

4.8 PERCENTAGE DIFFERENCE BETWEEN MAXIMUM TEMPERATURES OBTAINED THROUGH EXPERIMENT AND FEA FOR CARBIDE TOOL

Sl No	Feed (mm per rev)	Speed (rpm)	Machining Time (sec)	Depth of Cut (mm)	Max Expt Temp (°C)	Max FEA Temp (°C)	Percentage Difference (%)
1	0.52	150	49	0.1	75.4	77.02	2.10
2				0.4	111.8	115.03	2.81
3				0.7	159.4	162.05	1.64
4		420	17.5	0.1	82.8	85.025	2.62
5				0.4	119.2	117.04	6.36
6				0.7	167.6	169.06	0.86
7		710	10	0.1	86.8	90.027	3.58
8				0.4	127	129.04	1.58
9				0.7	175.2	174.06	0.65

Table 4.42 Percentage difference between max temperatures obtained for Carbide tool

CHAPTER 5
CONCLUSION

5.1 SUMMARY

Temperature at tool-chip interface of a single point cutting tool of High Speed Steel and Carbide Tip is determined, generated in a machining process at slow speed, medium speed and at high speed. Fluke IR Thermal Imager is used for measuring temperature at tool-chip interface. Single point cutting tool has been solid modelled by using SOLIDWORKS 2013 and Finite Element Analysis carried out by using ANSYS Workbench 15.

By varying speed and depth of cut, the effect of those on temperature are compared with the experimental results and FEA results. After comparison nearly 7% variation is found in between the results. Also the results reveal that the main factors responsible for increasing cutting temperature are cutting speed (v) and depth of cut (d) respectively.

5.2 CONCLUSION

1. Using ANOVA table, the speed is the most significant parameter followed by depth of cut for rising the temperature during machining.The percentage contribution obtained for HSS tool and Carbide tool as,

HSS tool - Speed: 70.25%, Depth of cut: 28.88%

Carbide tool - Speed: 69.86%, Depth of cut: 29.75%

2. Compared the results obtained from experiment and finite element analysis, the results were validated.The difference in temperature obtained for HSS tool and Carbide tool as,

HSS tool - not more than 4%

Carbide tool - not more than 7%

3. It can be observed that an increase of the cutting speed produces an increase of the cutting temperature. This result is due to the fact that an increase of the cutting speed

produces an increase of the cutting forces. More energy is needed to remove the material away increasing the cutting temperature.

4. It can be observed that an increase of the depth of cut produces an increase of the cutting temperature. When a material is plastically deformed, most of the energy is turned into heat since the material is subject to extremely severe deformations; being the elastic deformation the ones that represents a small part of the total deformation. Hence, the increase of depth of cut represents a bigger compression in the tool-work piece interface this will increase the energy supplied to the system during the cut of the material.

5. In both experiment and finite element analysis, the temperature formed during machining is more in carbide tool than in HSS tool. So the chances for tool wear or tool failure is more in carbide tool than in HSS tool at same cutting conditions.

5.3 SCOPE FOR FUTURE WORK

In this study, three different analyses are comparing to an experimental measurement of temperature in a machining process at slow speed, medium speed and at high speed. In addition, three analyses are done of a High Speed Steel and of a Carbide Tip Tool with Mild Steel machining process at three different cutting speeds and depth of cuts. Similarly we can use this analysis procedure for Different cutting tool and work piece combinations or for different tool geometries. Also we can analyse the machining by changing cutting conditions.

In this study, the finite element analysis was carried out by using ANSYS.It takes more computation time for the analysis. So for the same analysis we can use other simulation softwares for less computation time and better results.

CHAPTER 6

REFERENCES

[1] Shijun Zhang, Zhanqiang Liu, 2008. An analytical model for transient temperature distributions in coated carbide cutting tools International Communications in Heat and Mass Transfer 35, 1311–1315.

[2] L.B.ABHANG and M. HAMEEDULLAH, 2010. Chip-Tool Interface Temperature Prediction Model for Turning Process International Journal of Engineering Science and Technology Vol. 2(4), 382-393.

[3] J. E. JAM, V. N. FARD, 2011. A novel method to determine tool-chip thermal contact conductance in machining International Journal of Engineering Science and Technology (IJEST) ISSN: 0975-5462 Vol. 3 No.12.

[4] Yash R. Bhoyar, Asst. Prof. P. D. Kamble, 2013. Finite element analysis on temperature distribution in turning process using deform-3D International Journal of Research in Engineering and Technology ISSN: 2319-1163.

[5] Deepak Lathwal, Deepak Bhardwaj, 2013. Study and analysis of single point cutting tool under variable rake angle. Vol. 1 Issue I, ISSN: 2321-9653. International journal for research in applied science and engineering technology (IJRASET).

[6] Maheshwari N Patil, Shreepad Sarange, 2014.Numerical analysis to determine the distribution of tool forces and temperatures of single point cutting tool. International Journal of Science and Research (IJSR) ISSN (Online): 2319-7064.

[7] Meenu Sahu and Komesh Sah, 2014.Optimization of Cutting Parameters on Tool Wear, Work piece Surface Temperature and Material Removal Rate in Turning of AISI D2 Steel International Journal of Advanced Mechanical Engineering. ISSN 2250-3234 Volume 4, Number 3, pp. 291-298.

[8] S. H. Rathod, Mohd. Razik, 2014. Finite Element Analysis of Single Point Cutting Tool. IJMER | ISSN: 2249–6645 | Vol. 4 | Iss. 3 | 12 |.

[9] B. Fnides, M. A., Yallese, H. Aouici, 2008. Hard turning of hot works steel AISI H11: Evaluation of cutting pressures, resulting force and temperature ISSN 1392 - 1207. MECHANIKA.Nr.4 (72)

[10] Rogério Fernandes Brito, Solidônio Rodrigues de Carvalho, Sandro Metrevelle Marcondes de Lima e Silva, João Roberto Ferreira, 2009.Thermal analysis in coated cutting tools.International Communications in Heat and Mass Transfer 36, 314–321.

[11] R.K. Jain "A Text Book of Production Technology", Khanna Publishers.

[12] Cyril Donaldson, George H Lecain, V C Goold "A Text Book of Tool Design", McGraw Hill Publishers.

[13] KD Broota "A Text book of Experimental Design in Behavioural Research", Wiley eastern Ltd.

APPENDIX A

TABLE OF CRITICAL VALUES FOR THE F DISTRIBUTION

(0.01 SIGNIFICANCE LEVEL)

	1	2	3	4	5	6	7	8	9	10
1	4052.19	4999.52	5403.34	5624.62	5763.65	5858.97	5928.33	5981.10	6022.50	6055.85
2	98.50	99.00	99.17	99.25	99.30	99.33	99.36	99.37	99.39	99.40
3	34.12	30.82	29.46	28.71	28.24	27.91	27.67	27.49	27.35	27.23
4	21.20	18.00	16.69	15.98	15.52	15.21	14.98	14.80	14.66	14.55
5	16.26	13.27	12.06	11.39	10.97	10.67	10.46	10.29	10.16	10.05
6	13.75	10.93	9.78	9.15	8.75	8.47	8.26	8.10	7.98	7.87
7	12.25	9.55	8.45	7.85	7.46	7.19	6.99	6.84	6.72	6.62
8	11.26	8.65	7.59	7.01	6.63	6.37	6.18	6.03	5.91	5.81
9	10.56	8.02	6.99	6.42	6.06	5.80	5.61	5.47	5.35	5.26
10	10.04	7.56	6.55	5.99	5.64	5.39	5.20	5.06	4.94	4.85
11	9.65	7.21	6.22	5.67	5.32	5.07	4.89	4.74	4.63	4.54
12	9.33	6.93	5.95	5.41	5.06	4.82	4.64	4.50	4.39	4.30
13	9.07	6.70	5.74	5.21	4.86	4.62	4.44	4.30	4.19	4.10
14	8.86	6.52	5.56	5.04	4.70	4.46	4.28	4.14	4.03	3.94
15	8.68	6.36	5.42	4.89	4.56	4.32	4.14	4.00	3.90	3.81
16	8.53	6.23	5.29	4.77	4.44	4.20	4.03	3.89	3.78	3.69
17	8.40	6.11	5.19	4.67	4.34	4.10	3.93	3.79	3.68	3.59
18	8.29	6.01	5.09	4.58	4.25	4.02	3.84	3.71	3.60	3.51
19	8.19	5.93	5.01	4.50	4.17	3.94	3.77	3.63	3.52	3.43
20	8.10	5.85	4.94	4.43	4.10	3.87	3.70	3.56	3.46	3.37
21	8.02	5.78	4.87	4.37	4.04	3.81	3.64	3.51	3.40	3.31
22	7.95	5.72	4.82	4.31	3.99	3.76	3.59	3.45	3.35	3.26
23	7.88	5.66	4.77	4.26	3.94	3.71	3.54	3.41	3.30	3.21
24	7.82	5.61	4.72	4.22	3.90	3.67	3.50	3.36	3.26	3.17
25	7.77	5.57	4.68	4.18	3.86	3.63	3.46	3.32	3.22	3.13
26	7.72	5.53	4.64	4.14	3.82	3.59	3.42	3.29	3.18	3.09
27	7.68	5.49	4.60	4.11	3.79	3.56	3.39	3.26	3.15	3.06
28	7.64	5.45	4.57	4.07	3.75	3.53	3.36	3.23	3.12	3.03
29	7.60	5.42	4.54	4.05	3.73	3.50	3.33	3.20	3.09	3.01
30	7.56	5.39	4.51	4.02	3.70	3.47	3.31	3.17	3.07	2.98
31	7.53	5.36	4.48	3.99	3.68	3.45	3.28	3.15	3.04	2.96
32	7.50	5.34	4.46	3.97	3.65	3.43	3.26	3.13	3.02	2.93

33	7.47	5.31	4.44	3.95	3.63	3.41	3.24	3.11	3.00	2.91
34	7.44	5.29	4.42	3.93	3.61	3.39	3.22	3.09	2.98	2.89
35	7.42	5.27	4.40	3.91	3.59	3.37	3.20	3.07	2.96	2.88
36	7.40	5.25	4.38	3.89	3.57	3.35	3.18	3.05	2.95	2.86
37	7.37	5.23	4.36	3.87	3.56	3.33	3.17	3.04	2.93	2.84
38	7.35	5.21	4.34	3.86	3.54	3.32	3.15	3.02	2.92	2.83
39	7.33	5.19	4.33	3.84	3.53	3.31	3.14	3.01	2.90	2.81
40	7.31	5.18	4.31	3.83	3.51	3.29	3.12	2.99	2.89	2.80
41	7.30	5.16	4.30	3.82	3.50	3.28	3.11	2.98	2.88	2.79
42	7.28	5.15	4.29	3.80	3.49	3.27	3.10	2.97	2.86	2.78
43	7.26	5.14	4.27	3.79	3.48	3.25	3.09	2.96	2.85	2.76
44	7.25	5.12	4.26	3.78	3.47	3.24	3.08	2.95	2.84	2.75
45	7.23	5.11	4.25	3.77	3.45	3.23	3.07	2.94	2.83	2.74
46	7.22	5.10	4.24	3.76	3.44	3.22	3.06	2.93	2.82	2.73
47	7.21	5.09	4.23	3.75	3.43	3.21	3.05	2.92	2.81	2.72
48	7.19	5.08	4.22	3.74	3.43	3.20	3.04	2.91	2.80	2.72
49	7.18	5.07	4.21	3.73	3.42	3.20	3.03	2.90	2.79	2.71
50	7.17	5.06	4.20	3.72	3.41	3.19	3.02	2.89	2.79	2.70
51	7.16	5.05	4.19	3.71	3.40	3.18	3.01	2.88	2.78	2.69
52	7.15	5.04	4.18	3.70	3.39	3.17	3.01	2.87	2.77	2.68
53	7.14	5.03	4.17	3.70	3.38	3.16	3.00	2.87	2.76	2.68
54	7.13	5.02	4.17	3.69	3.38	3.16	2.99	2.86	2.76	2.67
55	7.12	5.01	4.16	3.68	3.37	3.15	2.98	2.85	2.75	2.66
56	7.11	5.01	4.15	3.67	3.36	3.14	2.98	2.85	2.74	2.66
57	7.10	5.00	4.15	3.67	3.36	3.14	2.97	2.84	2.74	2.65
58	7.09	4.99	4.14	3.66	3.35	3.13	2.97	2.84	2.73	2.64
59	7.09	4.98	4.13	3.66	3.35	3.12	2.96	2.83	2.72	2.64
60	7.08	4.98	4.13	3.65	3.34	3.12	2.95	2.82	2.72	2.63
61	7.07	4.97	4.12	3.64	3.33	3.11	2.95	2.82	2.71	2.63
62	7.06	4.97	4.11	3.64	3.33	3.11	2.94	2.81	2.71	2.62
63	7.06	4.96	4.11	3.63	3.32	3.10	2.94	2.81	2.70	2.62
64	7.05	4.95	4.10	3.63	3.32	3.10	2.93	2.80	2.70	2.61
65	7.04	4.95	4.10	3.62	3.31	3.09	2.93	2.80	2.69	2.61
66	7.04	4.94	4.09	3.62	3.31	3.09	2.92	2.79	2.69	2.60
67	7.03	4.94	4.09	3.61	3.30	3.08	2.92	2.79	2.68	2.60
68	7.02	4.93	4.08	3.61	3.30	3.08	2.91	2.79	2.68	2.59
69	7.02	4.93	4.08	3.60	3.30	3.08	2.91	2.78	2.68	2.59
70	7.01	4.92	4.07	3.60	3.29	3.07	2.91	2.78	2.67	2.59
71	7.01	4.92	4.07	3.60	3.29	3.07	2.90	2.77	2.67	2.58
72	7.00	4.91	4.07	3.59	3.28	3.06	2.90	2.77	2.66	2.58
73	7.00	4.91	4.06	3.59	3.28	3.06	2.90	2.77	2.66	2.57
74	6.99	4.90	4.06	3.58	3.28	3.06	2.89	2.76	2.66	2.57